nature cell biology

Autoregulatory mechanism for dynactin control of processive and diffusive dynein transport

Suvranta K. Tripathy[1,4], Sarah J. Weil[2,3,4], Chen Chen[2,3], Preetha Anand[1], Richard B. Vallee[2,5,6] and Steven P. Gross[1,5,6]

Dynactin is the longest known cytoplasmic dynein regulator, with roles in dynein recruitment to subcellular cargo and in stimulating processive dynein movement. The latter function was thought to involve the N-terminal microtubule-binding region of the major dynactin polypeptide p150^{Glued}, although recent results disputed this. To understand how dynactin regulates dynein we generated recombinant fragments of the N-terminal half of p150^{Glued}. We find that the dynein-binding coiled-coil α-helical domain CC1B is sufficient to stimulate dynein processivity, which it accomplishes by increasing average dynein step size and forward-step frequency, while decreasing lateral stepping and microtubule detachment. In contrast, the immediate upstream coiled-coil domain, CC1A, activates a surprising diffusive dynein state. CC1A interacts physically with CC1B and interferes with its effect on dynein processivity. We also identify a role for the N-terminal portion of p150^{Glued} in coordinating these activities. Our results reveal an unexpected form of long-range allosteric control of dynein motor function by internal p150^{Glued} sequences, and evidence for p150^{Glued} autoregulation.

A single major form of cytoplasmic dynein plays critical roles in many aspects of cell movement, including vesicular, virus and nuclear transport, cell migration, nuclear import, and mitotic and meiotic chromosome movement. Dynein adapts to diverse functions through a number of regulatory factors, most notably dynactin, LIS1, NudE and NudEL (ref. 1). LIS1 increases dynein force output by prolonging stalling under load[2] and also acts as a clutch to control dynein movement[3]. Dynactin is a megadalton-sized multi-subunit complex[4] involved in dynein recruitment to subcellular cargo[5,6] and in promoting processive dynein travel along microtubules[7–9]. Despite the importance of the latter activity for neuronal viability and other aspects of basic cell physiology, its underlying mechanism remains unknown.

p150^{Glued} is the largest polypeptide component of dynactin, and is thought to be the principal active subunit, containing both dynein- and microtubule-binding sites[10–12] (Fig. 1a,b). The latter, near the p150^{Glued} amino terminus, targets dynactin to growing microtubule ends[13–15] and contributes to organization of the mitotic spindle[16] and initiation of retrograde axonal transport[17,18]. Antibody inhibition of the microtubule-binding region was reported to diminish dynactin stimulation of dynein processivity[7], suggesting that p150^{Glued} might act by stabilizing and prolonging the dynein–microtubule interaction. However, removal of the p150^{Glued} N terminus had no effect on travel distance for individual dynein molecules *in vitro* or for vesicular cargo *in vivo*[9,15,16]. Sequential truncations of p150^{Glued} through its coiled-coil domain CC1 produced a stepwise decrease in dynein processivity[9]. Despite a role for this region in dynein binding in vertebrate dyneins[10–12], dynein binding persisted in the truncated yeast dynactin complex[9]. Dynactin also contributes to coordinating kinesin and dynein activities *in vivo*[19,20], although whether this effect is direct is unknown.

We have now carried out detailed analysis of p150^{Glued} fragments to reconstitute dynactin regulatory activity and understand the mechanisms by which dynactin regulates dynein. We find that the N-terminal half of p150^{Glued} is sufficient to reconstitute stimulation of processive dynein travel along microtubules, as well as an additional form of behaviour, dynein diffusion on microtubules. We identify specific processivity and diffusivity subdomains of p150^{Glued} and test how dynein stepping behaviour contributes to these functions. In the course of this work we also identified previously unidentified autoregulatory interactions between p150^{Glued} subdomains, which reveals dynactin to be a highly complex regulatory machine.

RESULTS

Analysis of p150^{Glued} fragments

To elucidate the molecular basis for dynein regulation by dynactin we produced a series of p150^{Glued} fragments spanning the N-terminal 555 amino-acid residues, including the microtubule- and dynein-binding

[1]Department of Developmental and Cell Biology, University of California, Irvine, California 92697, USA. [2]Department of Pathology and Cell Biology, Columbia University. New York, New York 10032, USA. [3]Department of Biological Sciences, Columbia University New York, New York 10027, USA. [4]These authors contributed equally to this work. [5]These authors jointly supervised this work.
[6]Correspondence should be addressed to R.B.V. or S.P.G. (e-mail: rv2025@columbia.edu or sgross@uci.edu)

Received 14 July 2014; accepted 14 October 2014; published online 24 November 2014; DOI: 10.1038/ncb3063

© 2014 Macmillan Publishers Limited. All rights reserved.

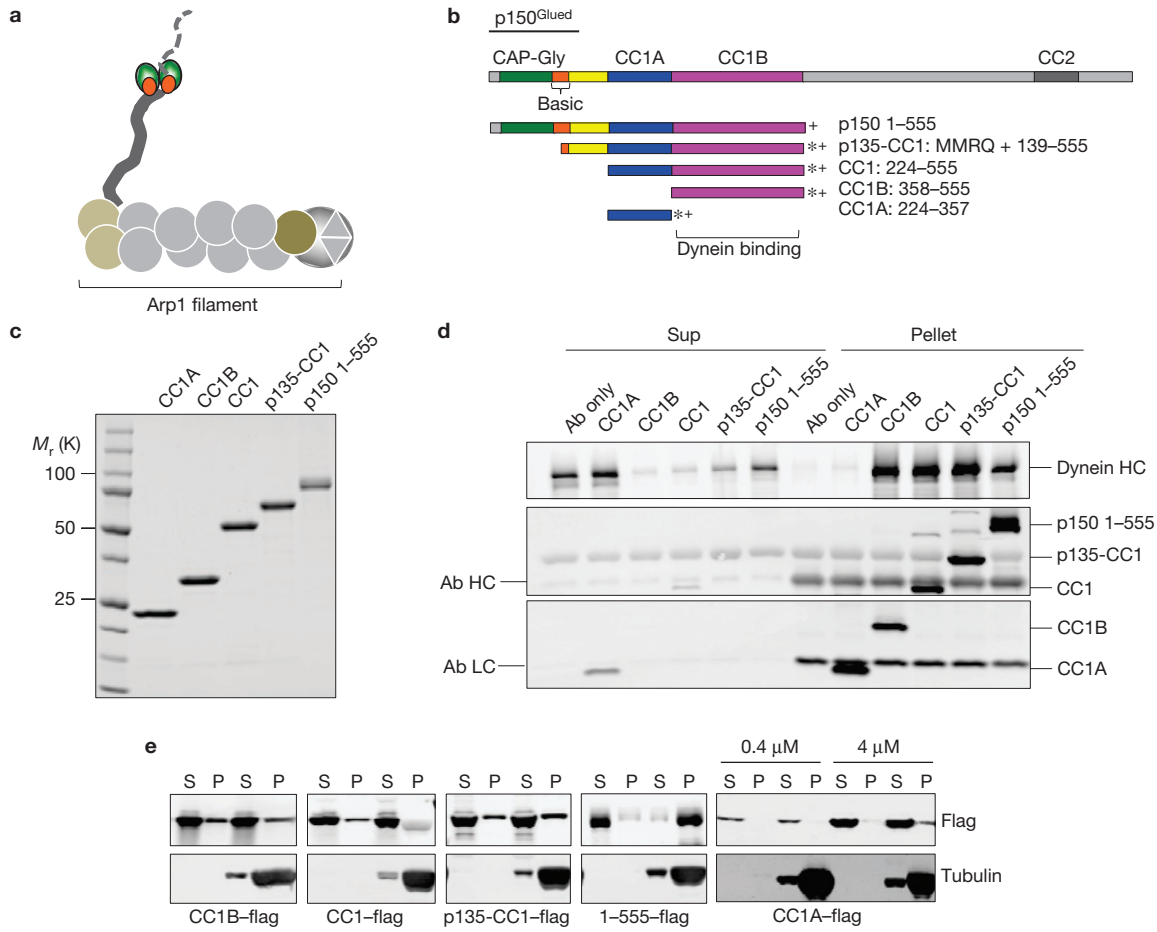

Figure 1 Characterization of dynactin p150^{Glued} fragments. (**a**) Diagram of the dynactin complex, an ~35-nm-long filament of the actin-like protein Arp1 and associated factors. The p150^{Glued} subunit is seen as a projecting arm at the left with globular N-terminal microtubule-binding CAP-Gly (green) and basic (orange) domains near the end. (**b**) Domain map of p150^{Glued} and its subfragments used in this study, which are C-terminally flag (*) and His_6 (+) tagged. CC1B and CC1A contain slightly different boundaries from those used in our previous study[21]. (**c**) Coomassie-stained gel of the purified p150^{Glued} fragments used in this study (3 independent experiments). (**d**) Calf brain cytoplasmic dynein was tested for co-immunoprecipitation with the Flag-tagged p150^{Glued} fragments using anti-flag antibody. Bands were visualized by western blotting with antibodies to dynein HC and the flag tag. All fragments except CC1A bound dynein (3 independent experiments). (**e**) Microtubule co-sedimentation of p150^{Glued} fragments. Fragments (0.1 μM, unless otherwise noted) were centrifuged in the absence or presence of taxol-stabilized microtubules. Only p150 1-555, which alone contains the CAP-Gly and complete basic regions of p150^{Glued}, showed substantial co-sedimentation with microtubules (2–3 independent experiments). CC: coiled-coil α-helix, Sup (S): supernatant, P: pellet, Ab: antibody. Uncropped images of blots are shown in Supplementary Fig. 6.

sites (Fig. 1b,c). This region is thought to be highly elongated, as suggested by its extensive predicted α-helical coiled-coil content. Electron microscopy has also revealed a pair of small globular elements presumed to contain the microtubule-binding domains towards the tip of a fine, projecting fibre, which may contain the predicted CC1 α-helical coiled-coil[4] (Fig. 1a,b). This structure is broken into two subregions, one of which, CC1B (refs 21,22), is responsible for binding to the dynein intermediate chains located within the tail portion of the dynein complex (Fig. 1a–d).

Each of the p150^{Glued} fragments showed no unexpected unfolding, as judged by physicochemical analysis (Supplementary Fig. 1 and Table 1). Analysis by circular dichroism spectroscopy showed substantial α-helical structure, suggested to be organized into a coiled-coil by a ratio of $\theta_{220}/\theta_{208} > 1$ (ref. 23; Supplementary Table 1). The fraction of α-helix in each fragment showed an approximate correspondence to the predicted coiled-coil content (Supplementary Table 1). CC1, CC1A and CC1B consisted largely of reversible, temperature-sensitive α-helical structure (Supplementary Fig. 1), as recently reported for similar fragments with slightly different boundaries[22].

Our largest p150^{Glued} fragment, p150 1–555, expressed using baculovirus, showed substantial microtubule binding, in contrast to the shorter fragments (Fig. 1e), consistent with a role for the N-terminal CAP-Gly and nearby basic domain of p150^{Glued} in microtubule binding[8,10,12]. All fragments containing CC1B pulled down purified calf brain cytoplasmic dynein, whereas CC1A did not (Fig. 1d).

Effects of p150^{Glued} fragments on single-molecule dynein behaviour

We used a laser trap bead assay to permit simultaneous analysis of both dynein force generation and transport along microtubules. Beads

© 2014 Macmillan Publishers Limited. All rights reserved.

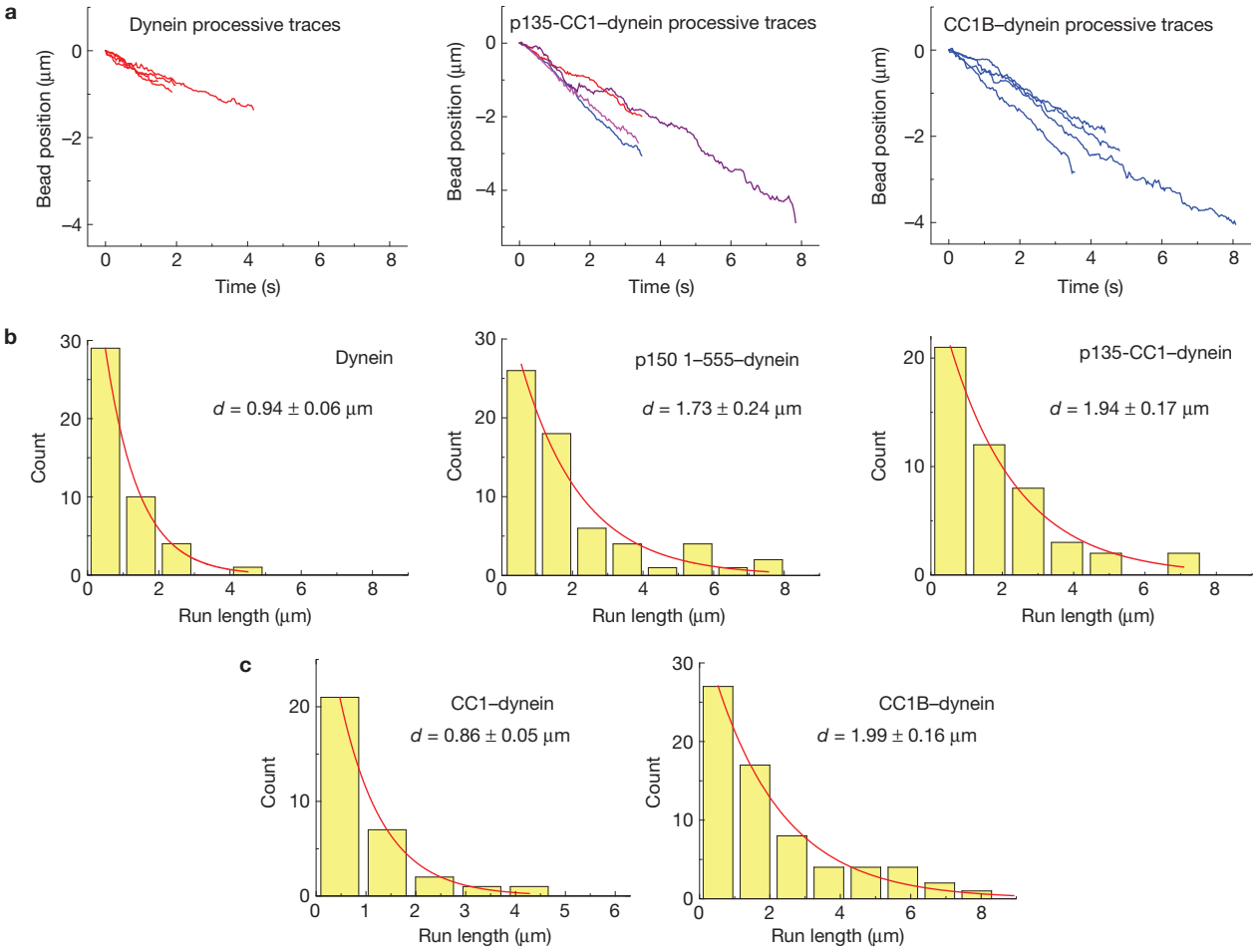

Figure 2 Effects of dynactin fragments on dynein-single-molecule processivity. (**a**) Sample traces (4 each) showing processive motion of beads with dynein alone (left) dynein plus p135-CC1 (middle) and dynein plus CC1B (right). (**b**) Bead-run-length distributions for dynein alone (left), dynein with P150 (middle), or dynein with P135 (right). (**c**) Run-length histograms for dynein with CC1 (left) and CC1B (right). In each case, data were well described by a single decaying exponential (chi-squared test) with mean travel for dynein plus the p150^{Glued} 1–555, p135-CC1 and CC1B fragments approximately double that for dynein alone (see also Table 1). All processivity measurements were carried out at a bead-binding fraction of ~30%.

adsorbed with the p150 1–555 fragment alone bound to microtubules and exhibited prolonged bidirectional motility ($\tau = 54.3 \pm 11$ s), determined to be diffusional ($D_0 = 0.069 \pm 10^{-4}$ μm^2 s^{-1}; Table 1) by mean square displacement analysis (Supplementary Fig. 2D). This behaviour is reminiscent of that for some previously characterized p150^{Glued} fragments[8] as well as for brain dynein–dynactin mixtures[24]. Beads adsorbed with the other p150^{Glued} fragments did not interact with microtubules.

To examine dynein behaviour, we adsorbed the motor protein to beads at single-molecule concentrations, blocked the beads with casein to prevent further protein recruitment, exposed them to a 150-fold molar excess of dynactin fragment, and washed them by centrifugation and re-suspension in motility buffer. We then captured individual beads using a laser trap, applied them to microtubules, determined stall force for the bound dynein, and then allowed the bead to travel freely along the microtubule (Supplementary Fig. 2A). Dynein alone showed predominantly processive behaviour (Fig. 2a and Table 1) associated with an average stall force of approximately 1.2 pN, corresponding to a single molecule[2,25] (Fig. 4a,b). This result is consistent with our earlier analysis[25] supporting processive movement for individual dynein molecules based on Poisson analysis of processivity as a function of motor dilution. As previously reported by us and others[25,26] some events were diffusive (Fig. 3a–c), as indicated by a linear mean square displacement plot (not shown, and Supplementary Fig. 2D–G). The ratio of processive to diffusive runs was generally high for our calf brain dynein (Fig. 3d,e,g), but varied among preparations and seemed to decrease with preparation age (Methods).

The addition of the p150^{Glued} fragment p150 1–555 had two effects: it increased the frequency of diffusive behaviour and the duration of both diffusive and processive behaviour (Figs 2b and 3e and Table 1). As the absolute bead-binding fraction was unchanged by the fragment (Table 1), the change in relative diffusive versus processive frequencies reflects a conversion from one form of behaviour to the other. Importantly, the average length for the processive runs was increased ~2.0-fold relative to that for dynein alone (Fig. 2b, middle; Table 1), very similar to the effect reported for the complete dynactin complex[7–9]. Stall forces for processively moving dynein beads exposed to p150 1–555 were again close to 1 pN

© 2014 Macmillan Publishers Limited. All rights reserved.

Table 1 Summary of single-molecule data.

	p150 1–555	Dynein	Dynein + p150 1–555	Dynein + p135-CC1	Dynein† + CC1	Dynein + CC1B	Dynein + CC1A	Dynein† + CC1A‡ (1:7,000)	Dynein + CC1A + CC1B
Binding fraction	N/A	N/A	Unaffected	Unaffected	Decreased (70% → 30%)	Unaffected	Unaffected	Decreased (34% → 17%)	Decreased (37% → 23%)
Processive beads	0%	83 ± 4%	70 ± 6%	50 ± 5%	30 ± 4%	83 ± 4%	83 ± 6%	0%	48 ± 6%
Run length (μm)	N/A	0.92 ± 0.09	1.84 ± 0.24	1.94 ± 0.17	0.86 ± 0.05	1.99 ± 0.16	0.76 ± 0.17	N/A	0.65 ± 0.05
Velocity ($\mu m\,s^{-1}$)	N/A	0.41 ± 0.04	0.24 ± 0.02	0.33 ± 0.03	0.24 ± 0.05	0.33 ± 0.03	0.28 ± 0.03	N/A	0.31 ± 0.04
Force (pN)	N/A*	1.18 ± 0.03	1.03 ± 0.02	1.09 ± 0.02	1.13 ± 0.02	1.2 ± 0.03	1.1 ± 0.02	N/A	1.05 ± 0.01
MT-binding time of processive beads (s)	N/A	2.7 ± 0.4	6.6 ± 0.8	5.4 ± 0.6	2.8 ± 0.4	5.2 ± 1	2.7 ± 0.6	N/A	2.8 ± 0.5
MT-binding time of diffusive beads (s)	54.3 ± 11	12.9 ± 2.07	29.8 ± 7.8	41.2 ± 9.4	8.2 ± 2	N/A	N/A	78.4 ± 13.6	3.5 ± 0.6
Diffusion coefficient of diffusive beads ($\mu m^2\,s^{-1}$)	0.07 ± 0.0001	0.017 ± 0.0002	0.04 ± 0.0015	0.018 ± 0.0003	0.0198 ± 0.0002	N/A	N/A	0.018 ± 0.000013	0.025 ± 0.00053

*$p150^{Glued}$ 1–555 alone or diffusive dynein motors do not generate force, as shown in Supplementary Fig. 3. Microtubule-associated transport properties of beads to which $p150^{Glued}$ 1–555 alone, cytoplasmic dynein alone, or dynein with $p150^{Glued}$ fragments were adsorbed. To test the effects of $p150^{Glued}$ fragments on dynein function, the motor protein was adsorbed at single-molecule concentrations, and the beads were blocked to prevent further protein binding, exposed to a 150-fold molar excess of fragment, centrifuged, and examined for motile behaviour in an optical trap. †CC1 and high concentrations of CC1A required increased dynein to maintain a 30% bead–microtubule binding fraction. Error is s.e.m. ‡CC1A was used at a 7,000-fold molar excess over dynein and remained present during motility analysis.

(Fig. 4b and Supplementary Fig. 2), and stall duration was prolonged (Fig. 4a,b, right).

In addition to their greater relative frequency, (Fig. 3e), the duration of diffusive dynein events was prolonged by ~3-fold (Table 1). The diffusion coefficient was smaller than that for $p150^{Glued}$ 1–555 alone (Supplementary Fig. 2F), but greater than that for dynein, suggesting that at least a component of the observed diffusion is associated with the dynein–microtubule interaction. The diffusing beads produced minimal force (see Supplementary Fig. 3 and Methods), with small force peaks at 0 ± 0.35–0.5 pN, behaviour that was not seen for trapped beads diffusing in the trap without a motor (Supplementary Fig. 3 and Methods). The minimal motor effects probably reflect random binding to microtubules and release, rather than directed motion, because their magnitude is consistent with thermal noise without the motor (Supplementary Fig. 3A, right), and because individual trajectories (Supplementary Fig. 3F,I) show sudden decreases in thermal motion, rather than obvious binding and subsequent directed transport. The observation of genuine diffusive and processive states, and the dynactin-induced changes in their relative frequency and properties, suggested that the dynein regulatory activity of the complete dynactin complex resides substantially within the N-terminal half of $p150^{Glued}$, encouraging us to search further for specific regulatory loci.

The p135-CC1 fragment was designed to correspond to the N terminus of a naturally occurring $p150^{Glued}$ splice variant lacking the CAP-Gly domain and most of the basic region[27]. Remarkably, when combined with dynein, p135-CC1 had effects similar to those of p150 1–555, again increasing the frequency of diffusive events (Fig. 3d), as well as the duration of both processive and diffusive microtubule interactions (Figs 2 and 3 and Table 1). As p135-CC1 does not show significant microtubule binding (Fig. 1e), its effect on diffusion must result from changes to dynein behaviour (Supplementary Fig. 2G). The absence of the microtubule-binding CAP-Gly and basic regions in p135-CC1 reveals further that these regions are dispensable for regulating dynein processivity as well as diffusion. For the diffusive beads, force production was again minimal (Supplementary Fig. 3H–J). Dynein in this state could easily be displaced along microtubules at the lowest optical trap setting (<0.4 pN), although lateral detachment required higher forces (data not shown). Thus, these data demonstrate that dynactin can actually turn off dynein force production, a previously unidentified regulatory function, while allowing dynein to retain its interaction with microtubules.

In contrast to these results, the CC1 fragment severely inhibited the dynein–microtubule interaction, requiring a 2.3-fold increase in dynein concentration to achieve an equivalent number of microtubule-binding events. CC1 inhibition reflected a selective decrease in the frequency of processive events (Fig. 3f), as the absolute number of diffusive microtubule interactions was unchanged. These results together revealed CC1 to have a potent inhibitory effect on processive dynein motion, despite the presence in this fragment of the dynein-binding portion of $p150^{Glued}$. This observation has relevance for the long-standing use of CC1 in cell expression studies as a potent dynein inhibitor[28]. Although part of its effect seems due to its ability to compete with both dynactin and NudE–LIS1 for dynein binding[21,29], our current results identify an additional direct toxic effect on dynein function.

© 2014 Macmillan Publishers Limited. All rights reserved.

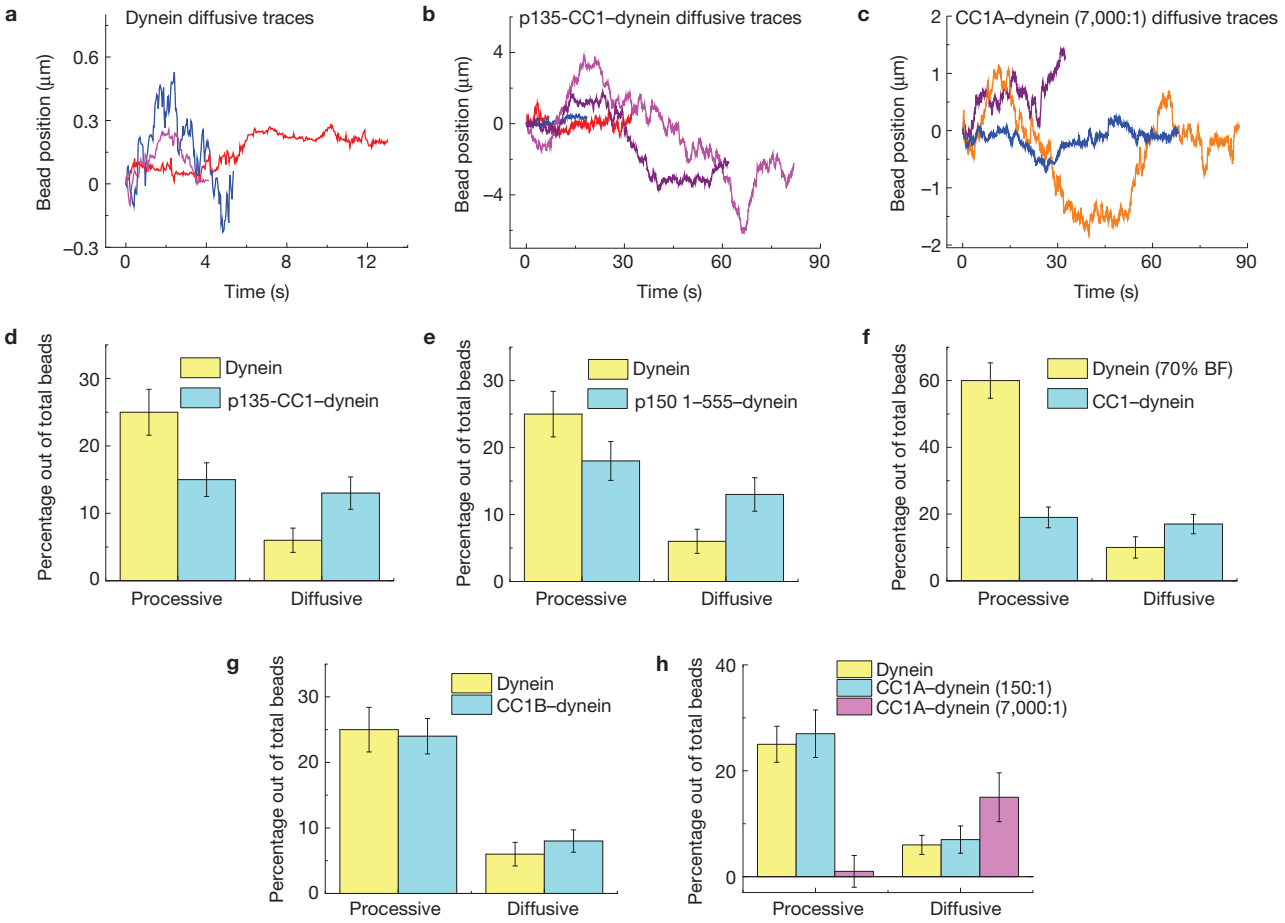

Figure 3 Effects of dynactin fragments on dynein single-molecule diffusivity. (**a**–**c**) Sample traces (3–4) showing diffusive motion of beads with dynein alone (**a**), dynein with p135-CC1 (**b**) and dynein with high amounts of CC1A (**c**). (**d**–**h**) Quantification of the effects of different dynactin fragments on the overall amount of diffusive versus processive binding events. As the percentage of dynein-alone diffusion could change between experiments, each graph reports the results of the control (dynein-alone) performed at the same time as the fragment experiment. The sum of the diffusive and processive components reflects the total bead-binding fraction (for example, in **d**, the total bead-binding fraction for dynein alone was 30%). P135 (**d**) and P150 (**e**) decreased the gross number of processive events, and increased the number of diffusive events. CC1 (**f**) decreased the gross number of processive events, but did not increase diffusive events, and CC1B (**g**) did not alter the number of either class of events. CC1A (**h**) had no effect at low concentrations, but induced diffusion and suppressed processive motion at high concentrations. These data reflect numerous experiments. Error bars (Fig. 3d–h) were obtained using equation $\sqrt{P*(1-P)/N}$, where P refers to bead-binding fraction and N refers to the total number of beads tested. For dynein alone, dynein–p135-CC1, dynein–p150 1–555, dynein–CC1B, dynein–CC1 (70% BF), dynein–CC1A (150:1) and dynein–CC1A (7,000:1), the respective number of beads checked was $N = 165$, 195, 180, 253, 161, 70 and 70. For high dynein (70% BF), $N = 85$. Each experiment was reproduced in the laboratory at least 3 times. The single-dynein-alone control experiment was repeated before each measurement of dynein with a dynactin fragment.

Distinct p150^{Glued} processivity- and diffusivity-enhancing domains

To identify subdomains responsible for dynactin regulation of dynein and the unexpected inhibitory effects of CC1, we examined smaller p150^{Glued} fragments. Strikingly, CC1B induced a clear 2.2-fold increase in dynein run length (Fig. 2a right, Fig. 2c, middle; Table 1) but did not change the frequency of either processive or diffusive events (Fig. 3g). The magnitude of the effect on run lengths was similar to values observed for the entire dynactin complex[7,9] and to that for the longer p150^{Glued} fragments characterized in this study (Table 1 and Fig. 2). The results support a role for the CC1 region reported in yeast[9] although our analysis of CC1 (above) and CC1A (below) reveals clear differences from the yeast work. Dynein force production was normal (Fig. 4), confirming single-motor behaviour. These results identified CC1B as the processivity-stimulating domain of p150^{Glued}.

To gain insight into the mechanism responsible for this activity we evaluated dynein stepping along microtubules, combining a force-feedback optical trap with a new step-detection approach (see Methods and Supplementary Fig. 4 and Table 2). The motor protein alone exhibited a mix of step sizes. Forward 8 nm steps predominated (Fig. 5a–c and Supplementary Table 2), although reverse and lateral steps were also observed, as previously reported[30–32] (Fig. 5c–g). CC1B altered each of these behaviours, causing a higher proportion of forward to reverse steps, an increase in forward-step size and a decreased frequency and size of lateral steps (Fig. 5 and Supplementary Figs 4 and 5 and Supplementary Table 2 and Methods). The average step size increased from 6.28 to

© 2014 Macmillan Publishers Limited. All rights reserved.

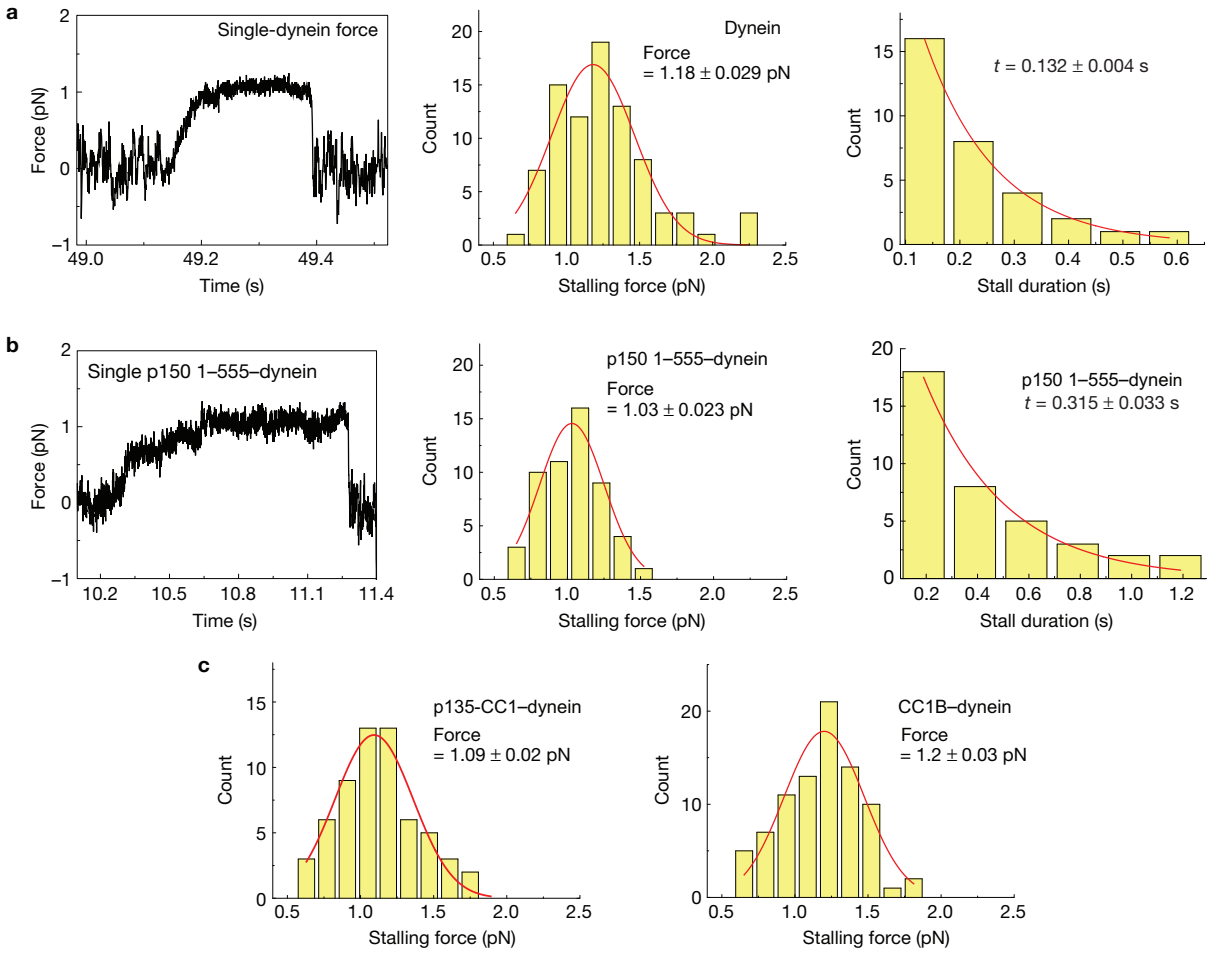

Figure 4 Effects of dynactin fragments on dynein-single-molecule force production. (**a**) Dynein alone. (**b**) Dynein with P150. Shown are example force traces (**a**,**b**, left), distributions of stalling forces (100 force events; **a**,**b**, middle) and distributions of durations of force producing events (40 stalling events; **a**,**b**, right). (**c**) Distributions of stalling forces for dynein with p135 (left) and CC1B (right).

11.22 nm (Methods), corresponding to a predicted 1.8-fold increase in travel distance, slightly less than the experimentally observed 2-fold increase. The remaining increase reflects a decreased probability of detachment per step (average of 177 steps with CC1B versus 146 for dynein alone). Our observations, thus, identify a mechanism for dynein processivity regulation independent of the N-terminal $p150^{Glued}$ microtubule-binding region, and involving changes to stepping behaviour.

We next examined CC1A, which, at low concentrations, had a minimal effect on dynein behaviour (Fig. 3h and Table 1). At a very high ratio to dynein (7,000:1), CC1A reduced dynein interactions with microtubules (Fig. 3h and Table 1). Strikingly, all motile events were diffusive (Fig. 3c,h and Supplementary Fig. 2D), with minimal force production. CC1A, thus, promotes the diffusional dynein state exclusively. CC1A binding to dynein cannot be readily detected by biochemical means (Fig. 1), and must, therefore, involve a weak, transient interaction, as discussed below. We note that the diffusion coefficient for dynein in the presence of CC1A or p135-CC1 is comparable to that for dynein alone (Table 1), suggesting that dynein has the same interaction with the microtubules in each case, although the duration of diffusive events is increased by these $p150^{Glued}$ fragments. CC1A and larger CC1A-containing fragments showed little evidence of microtubule binding (Fig. 1e), suggesting that the CC1A region may directly stabilize dynein in an inherent diffusive conformation.

Interaction between CC1A and CC1B

Dynein inhibition by CC1 differs from the effects of its CC1A and CC1B subfragments alone, suggesting a potential cooperative interaction between them. Indeed, we observed clear evidence that GST–CC1A binds CC1B in pull-down assays (Fig. 6a). We also tested for cofractionation of CC1A and CC1B by size-exclusion fast protein liquid chromatography (FPLC), and found clear evidence for a shift to a greater hydrodynamic radius for the combined fragments relative to each alone (Fig. 6b). To test for an effect on motor behaviour we exposed beads sequentially to dynein, CC1B and CC1A, the last of these at a 150-fold molar excess relative to dynein. At this ratio CC1A alone has minimal effect on dynein (Table 1). However, it clearly suppressed CC1B enhancement, decreasing the overall frequency of processive motion (Fig. 6c) and mean travel distance (Fig. 6d).

© 2014 Macmillan Publishers Limited. All rights reserved.

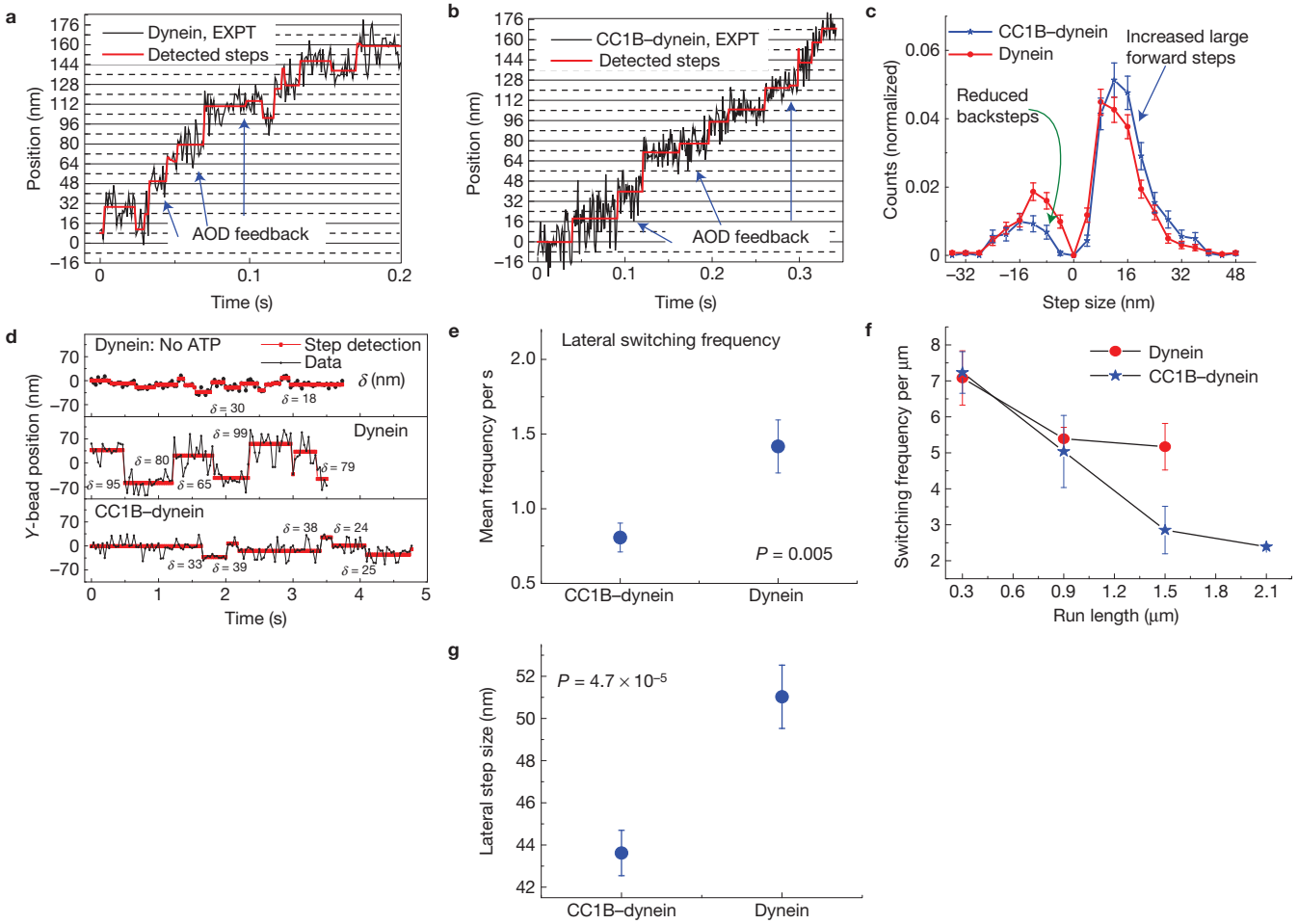

Figure 5 Effects of processivity-enhancing fragment CC1B on dynein stepping behaviour. (**a**,**b**) Sample dynein bead traces with detected steps (in red) for single dynein alone (**a**) and with CC1B (**b**). Arrows indicate points of force feedback (Methods). (**c**) Distribution of step sizes for single dyneins with (blue) or without (red) CC1B (428 stepping events). CC1B reduces back-stepping (green arrow) and increases large forward steps (blue arrow). (**d**) Sample traces showing lateral bead position on microtubule versus time for stationary dynein (without ATP-top); and dynein alone (middle) or with CC1B (bottom) moving on a microtubule in the presence of saturating ATP. Step detection identifies changes in lateral bead position (red lines); δ indicates size of detected lateral step in nanometres. (**e**,**f**) Lateral dynein bead switching frequency (95 switching events) on the microtubule surface (**e**), and as a function of run length (94 run lengths; **f**); P value from t-test. Longer CC1B–dynein runs correlate with decreased lateral switching frequency. (**g**) Magnitude of lateral step size (428 detected steps). CC1B decreases the frequency and magnitude of lateral dynein steps. Error bars are s.e.m.

These results thus identify a direct interaction between CC1A and CC1B, and reveal that CC1A inhibits the functional effects of the CC1B–dynein interaction (Fig. 6d). The net outcome is similar to the effects of CC1, suggesting that its subdomains are capable of interacting to regulate each other. The observation that CC1 binds dynein, but inhibits its motility, suggests that its CC1B subdomain remains associated with dynein when dynactin is in either a stimulatory or inhibitory conformational state.

DISCUSSION

These results indicate that the subdomains of CC1 have the remarkable ability to modulate processive and diffusive dynein behaviour. However, in either covalent or non-covalent combination with CC1A, the effect of CC1B on dynein processivity is suppressed. Thus, CC1 alone cannot completely account for the dynein regulatory properties of dynactin. Instead, our results argue for further intramolecular regulation by the N-terminal globular region of p150^{Glued} or p135. Fragments including the globular domain stimulate both processivity and diffusivity, and mimic the effects of the complete dynactin complex. Thus, the globular domain must suppress the inhibitory effect of CC1A, further modulating its behaviour. Although the structural organization of p150^{Glued} within the complete dynactin complex remains incompletely understood, we speculate that CC1 must be capable of folding on itself to allow CC1A and CC1B to interact (Fig. 6e). In fact, recent electron microscopy analysis of dynactin shows CC1A and CC1B to behave as a hairpin structure at the tip of the dynactin projection (Y. Toyoshima, personal communication), consistent with this possibility. We note further that, as CC1A is substantially shorter than CC1B, this arrangement would allow the N-terminal globular domain of p150^{Glued} or p135 to contact the C-terminal portion of CC1B, and, perhaps, further modulate its behaviour. The globular N-terminal region is known to bind to microtubules and other interactors[33]. On the basis of our current data, we speculate that

© 2014 Macmillan Publishers Limited. All rights reserved.

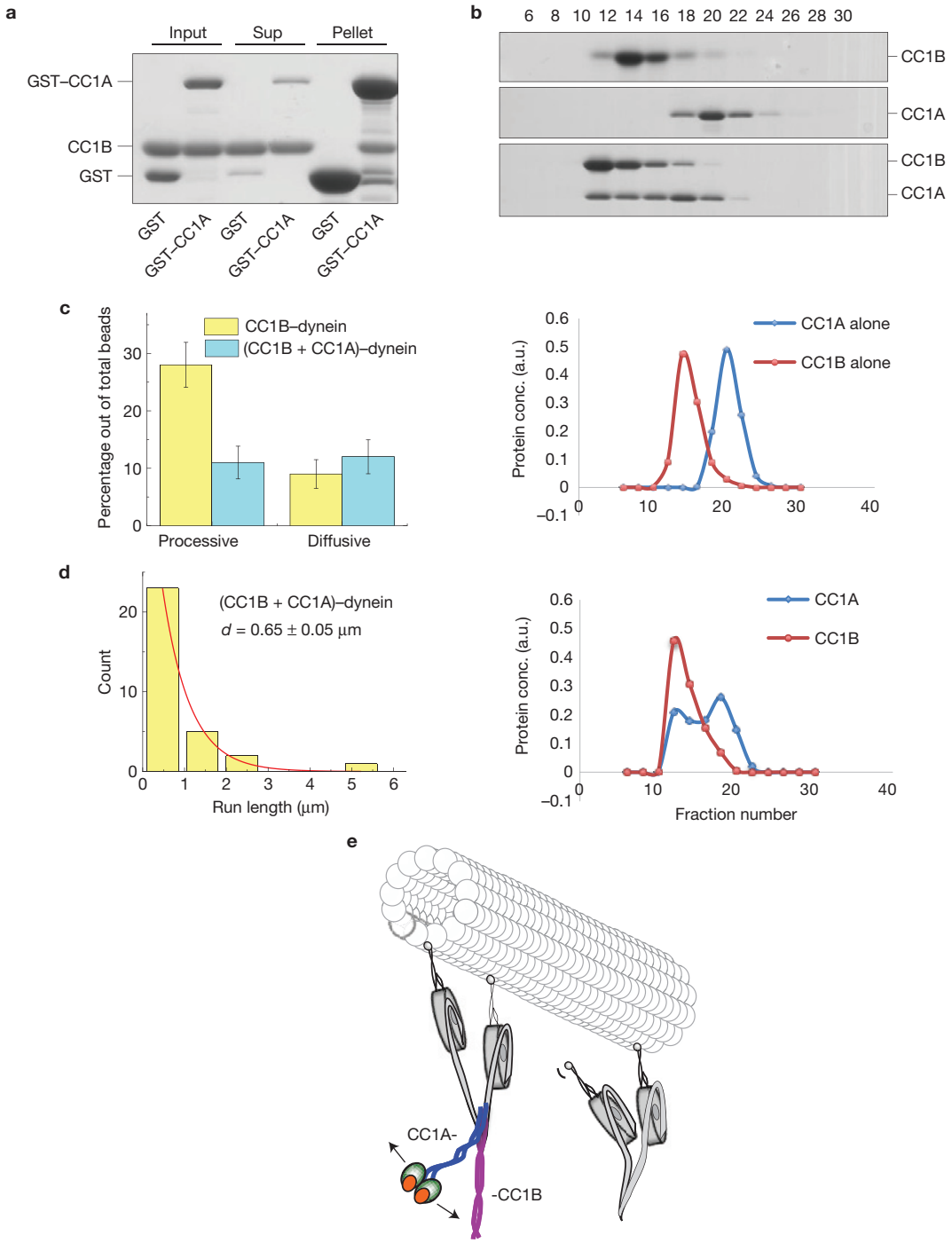

Figure 6 Interaction between coiled-coil p150^{Glued} fragments CC1A and CC1B. (**a**) Pulldown of bacterially expressed CC1B with GST–CC1A or GST alone shows specific binding of CC1B to CC1A using Coomassie blue staining (3 independent experiments). (**b**) Size-exclusion FPLC of CC1A and CC1B using Coomassie blue staining (3 independent experiments). When in combination the two fragments elute in a common, higher-molecular-size peak. (**c**,**d**) Single-molecule bead assays reveal that CC1A, at a level that has no effect on its own on dynein (150:1 CC1A/dynein), strongly suppresses the effect of CC1B on dynein (see the caption of Fig. 3 for the number of beads checked). The number of processive dynein events and their average run length are reduced relative to values for dynein alone, suggesting that, as for CC1, the combined fragments actively inhibit dynein function. Error is s.e.m. (**e**) Schematic representation of dynein regulation by dynactin. (Left) Dimer of p150^{Glued} N terminus (amino acids 1–555) binds through its CC1B coiled-coil domain with the dynein intermediate chains situated within the dynein tail. CC1B alone is sufficient to increase the length of processive dynein movement along microtubules. CC1A is shown interacting physically with CC1B. As the two domains are covalently linked in the intact p150^{Glued} and p135 polypeptides, we propose that CC1 must bend as shown. In this conformation, the N-terminal globular portion of p150^{Glued} and p135 might be able to interact with the C-terminal portion of CC1B. Thus, we envision a series of intramolecular interactions within p150^{Glued} or p135, ultimately modulating dynein behaviour through its tail domain. We propose that the ultimate target of regulation is the dynein motor domains, the behaviour of which seems more clearly coordinated in the presence of the dynactin fragments, as evidenced by more efficient stepping along microtubules and longer runs. Uncropped images of blots are shown in Supplementary Fig. 6.

© 2014 Macmillan Publishers Limited. All rights reserved.

the N-terminal regions of p150^{Glued} and of p135 may, in turn, modulate interactions between CC1A and CC1B, and between the latter and dynein.

The only known site for this interaction is within dynein in the N-terminal 44 residues of the intermediate chain[21,22,29] (IC), which is a major component of the dynein tail. Our data, therefore, suggest that dynactin regulation involves very long-range communication between the dynein tail and motor domains, resulting in improved motor coordination. A related mechanism but with an opposite effect on motor activity was identified by analysis of dynein purified from the *Loa* mutant mouse[30]. We found in this case that a mutation in the tail portion of the dynein heavy chain (HC) specifically inhibits processivity, with an increase in wandering behaviour on the microtubule surface. Recent results in the yeast *Saccharomyces cerevisiae* showed further that deletion of the dynein light chain (LC) subunit weakens the IC–HC interaction, as was seen in *Loa* dynein, again decreasing processivity[34]. Together, these results suggest a common regulatory mechanism inhibited by the *Loa* mutation but stimulated by dynactin, probably mediated through components of the dynein IC–LC complex. Our results support findings that, within the cytoplasmic dynein dimer, the motor domains are inefficiently coordinated[31,32] and suggest that dynactin may act to increase motor coordination through a long-range allosteric mechanism. The effects on motor behaviour are manifested in increasing average forward-step size, suppressing backward steps, and decreasing overall probability of motor detachment from the microtubule per step.

Our data also identify mechanisms for switching dynein between processive and diffusive states. Such behaviour has recently been reported for individual fluorescently tagged dynein molecules in the yeast *Schizosaccharomyces pombe*. Dynein exhibited one-dimensional diffusion along cytoplasmic microtubules to reach Num1 cortical anchorage sites, after which the dynein exhibited directed, processive movement[35]. Expression of the dynein-binding portion of Num1, which interacts with the base of the complex[36], converted dynein from diffusive to processive behaviour. Our results identify dynactin as a physiological dynein regulator capable of inducing what may be equivalent states. We speculate that in different contexts, the ability of dynactin to turn off dynein force production could play a role in minimizing tug-of-war interactions between kinesin and dynein[19,20] in the cell.

Recent studies have identified a family of RDD (Rab–dynein–dynactin)-binding adapters[37] capable of strongly stimulating dynactin-mediated cytoplasmic dynein processivity[38,39]. Whether these factors act simply as scaffolds to facilitate the weak dynein–dynactin interaction[40], or, instead, upregulate the mechanism discovered in our current study remains an important question for future investigation. We note that dynein used in the recent studies[38,39] exhibited very limited processivity. The use of beads as in the current work not only allows dynein force production to be determined, but also enables higher-resolution spatial tracking than is possible with fluorescently tagged motors at present, and has revealed mammalian dynein to be clearly processive[25,30]. We note that the length of runs detected in the current *in vitro* assays are also more representative of the behaviour of physiological cargo *in vivo*[41,42]. Thus, the generality of RDD adapter function among cargo forms, and how their behaviour may be modulated, remain additional questions for further research.

METHODS

Methods and any associated references are available in the online version of the paper.

Note: Supplementary Information is available in the online version of the paper

ACKNOWLEDGEMENTS

We thank R. McKenney for help in initiating this project and A. Baffet for helpful comments on the manuscript. Support by GM102347 to R.B.V. and GM070676 to S.P.G.

AUTHOR CONTRIBUTIONS

R.B.V., S.P.G., S.J.W. and S.K.T. designed experiments; S.K.T., S.J.W. and C.C. performed the experiments; P.A. provided kinesin; R.B.V., S.P.G., S.K.T., C.C. and S.J.W. wrote the paper.

COMPETING FINANCIAL INTERESTS

The authors declare no competing financial interests.

Published online at www.nature.com/doifinder/10.1038/ncb3063
Reprints and permissions information is available online at www.nature.com/reprints

1. Vallee, R. B., McKenney, R. J. & Ori-McKenney, K. M. Multiple modes of cytoplasmic dynein regulation. *Nat. Cell Biol.* **14,** 224–230 (2012).
2. McKenney, R. J., Vershinin, M., Kunwar, A., Vallee, R. B. & Gross, S. P. LIS1 and NudE induce a persistent dynein force-producing state. *Cell* **141,** 304–314 (2010).
3. Huang, J., Roberts, A. J., Leschziner, A. E. & Reck-Peterson, S. L. Lis1 acts as a "Clutch" between the ATPase and microtubule-binding domains of the dynein motor. *Cell* **150,** 975–986 (2012).
4. Schroer, T. A. Dynactin. *Annu. Rev. Cell Dev. Biol.* **20,** 759–779 (2004).
5. Echeverri, C. J., Paschal, B. M., Vaughan, K. T. & Vallee, R. B. Molecular characterization of the 50-kD subunit of dynactin reveals function for the complex in chromosome alignment and spindle organization during mitosis. *J. Cell Biol.* **132,** 617–633 (1996).
6. Holleran, E. A., Tokito, M. K., Karki, S. & Holzbaur, E. L. Centractin (ARP1) associates with spectrin revealing a potential mechanism to link dynactin to intracellular organelles. *J. Cell Biol.* **135,** 1815–1829 (1996).
7. King, S. J. & Schroer, T. A. Dynactin increases the processivity of the cytoplasmic dynein motor. *Nat. Cell Biol.* **2,** 20–24 (2000).
8. Culver-Hanlon, T. L., Lex, S. A., Stephens, A. D., Quintyne, N. J. & King, S. J. A microtubule-binding domain in dynactin increases dynein processivity by skating along microtubules. *Nat. Cell Biol.* **8,** 264–270 (2006).
9. Kardon, J. R., Reck-Peterson, S. L. & Vale, R. D. Regulation of the processivity and intracellular localization of *Saccharomyces cerevisiae* dynein by dynactin. *Proc. Natl Acad. Sci. USA* **106,** 5669–5674 (2009).
10. Holzbaur, E. L. F. *et al.* Homology of a 150K cytoplasmic dynein-associated polypeptide with the *Drosophila* gene Glued. *Nature* **351,** 579–583 (1991).
11. Vaughan, K. T. & Vallee, R. B. Cytoplasmic dynein binds dynactin through a direct interaction between the intermediate chains and p150Glued. *J. Cell Biol.* **131,** 1507–1516 (1995).
12. Waterman-Storer, C. M., Karki, S. & Holzbaur, E. L. The p150Glued component of the dynactin complex binds to both microtubules and the actin-related protein centractin (Arp-1). *Proc. Natl Acad. Sci. USA* **92,** 1634–1638 (1995).
13. Vaughan, P. S., Miura, P., Henderson, M., Byrne, B. & Vaughan, K. T. A role for regulated binding of p150(Glued) to microtubule plus ends in organelle transport. *J. Cell Biol.* **158,** 305–319 (2002).
14. Watson, P. & Stephens, D. J. Microtubule plus-end loading of p150Glued is mediated by EB1 and CLIP-170 but is not required for intracellular membrane traffic in mammalian cells. *J. Cell Sci.* **119,** 2758–2767 (2006).
15. Dixit, R., Levy, J. R., Tokito, M., Ligon, L. A. & Holzbaur, E. L. F. Regulation of dynactin through the differential expression of p150(Glued) isoforms. *J. Biol. Chem.* **283,** 33611–33619 (2008).
16. Kim, H. *et al.* Microtubule binding by dynactin is required for microtubule organization but not cargo transport. *J. Cell Biol.* **176,** 641–651 (2007).
17. Moughamian, A. J. & Holzbaur, E. L. Dynactin is required for transport initiation from the distal axon. *Neuron* **74,** 331–343 (2012).
18. Lloyd, T. E. *et al.* The p150(Glued) CAP-Gly domain regulates initiation of retrograde transport at synaptic termini. *Neuron* **74,** 344–360 (2012).
19. Gross, S. P., Welte, M. A., Block, S. M. & Wieschaus, E. F. Coordination of opposite-polarity microtubule motors. *J. Cell Biol.* **156,** 715–724 (2002).
20. Haghnia, M. *et al.* Dynactin is required for coordinated bidirectional motility, but not for dynein membrane attachment. *Mol. Biol. Cell* **18,** 2081–2089 (2007).
21. McKenney, R. J., Weil, S. J., Scherer, J. & Vallee, R. B. Mutually exclusive cytoplasmic dynein regulation by NudE-Lis1 and dynactin. *J. Biol. Chem.* **286,** 39615–39622 (2011).
22. Siglin, A. E. *et al.* Dynein and dynactin leverage their bivalent character to form a high-affinity interaction. *PLoS ONE* **8,** e59453 (2013).

© 2014 Macmillan Publishers Limited. All rights reserved.

23. Lau, S. Y., Taneja, A. K. & Hodges, R. S. Synthesis of a model protein of defined secondary and quaternary structure. Effect of chain length on the stabilization and formation of two-stranded alpha-helical coiled-coils. *J. Biol. Chem.* **259,** 13253–13261 (1984).
24. Ross, J. L., Wallace, K., Shuman, H., Goldman, Y. E. & Holzbaur, E. L. F. Processive bidirectional motion of dynein–dynactin complexes *in vitro*. *Nat. Cell Biol.* **8,** 562–570 (2006).
25. Mallik, R., Carter, B. C., Lex, S. A., King, S. J. & Gross, S. P. Cytoplasmic dynein functions as a gear in response to load. *Nature* **427,** 649–652 (2004).
26. Wang, Z., Khan, S. & Sheetz, M. P. Single cytoplasmic dynein molecule movements: characterization and comparison with kinesin. *Biophys. J.* **69,** 2011–2023 (1995).
27. Tokito, M. K., Howland, D. S., Lee, V. M. & Holzbaur, E. L. Functionally distinct isoforms of dynactin are expressed in human neurons. *Mol. Biol. Cell* **7,** 1167–1180 (1996).
28. Quintyne, N. J. *et al.* Dynactin is required for microtubule anchoring at centrosomes. *J. Cell Biol.* **147,** 321–334 (1999).
29. Morgan, J. L., Song, Y. & Barbar, E. Structural dynamics and multiregion interactions in dynein–dynactin recognition. *J. Biol. Chem.* **286,** 39349–39359 (2011).
30. Ori-McKenney, K. M., Xu, J., Gross, S. P. & Vallee, R. B. A cytoplasmic dynein tail mutation impairs motor processivity. *Nat. Cell Biol.* **12,** 1228–1234 (2010).
31. DeWitt, M. A., Chang, A. Y., Combs, P. A. & Yildiz, A. Cytoplasmic dynein moves through uncoordinated stepping of the AAA+ ring domains. *Science* **335,** 221–225 (2012).
32. Qiu, W. *et al.* Dynein achieves processive motion using both stochastic and coordinated stepping. *Nat. Struct. Mol. Biol.* **19,** 193–200 (2012).
33. Weisbrich, A. *et al.* Structure–function relationship of CAP-Gly domains. *Nat. Struct. Mol. Biol.* **14,** 959–967 (2007).
34. Rao, L. *et al.* The yeast dynein Dyn2-Pac11 complex is a dynein dimerization/processivity factor: structural and single-molecule characterization. *Mol. Biol. Cell* **24,** 2362–2377 (2013).
35. Ananthanarayanan, V. *et al.* Dynein motion switches from diffusive to directed upon cortical anchoring. *Cell* **153,** 1526–1536 (2013).
36. Tang, X., Germain, B. S. & Lee, W-L. A novel patch assembly domain in Num1 mediates dynein anchoring at the cortex during spindle positioning. *J. Cell Biol.* **196,** 743–756 (2012).
37. Scherer, J, Yi, J. & Vallee, R. B. PKA-dependent dynein cargo switching from lysosomes to adenovirus: a novel form of host-virus competition. *J. Cell Biol.* **205,** 163–177 (2014).
38. Schlager, M. A., Hoang, H. T., Urnavicius, L., Bullock, S. L. & Carter, A. P. *In vitro* reconstitution of a highly processive recombinant human dynein complex. *EMBO J.* **33,** 1855–1868 (2014).
39. McKenney, R. J., Huynh, W., Tanenbaum, M. E., Bhabha, G. & Vale, R. D. Activation of cytoplasmic dynein motility by dynactin-cargo adapter complexes. *Science* **345,** 337–341 (2014).
40. Paschal, B. M. *et al.* Characterization of a 50-kDa polypeptide in cytoplasmic dynein preparations reveals a complex with p150GLUED and a novel actin. *J. Biol. Chem.* **268,** 15318–15323 (1993).
41. Yi, J. Y. *et al.* High-resolution imaging reveals indirect coordination of opposite motors and a role for LIS1 in high-load axonal transport. *J. Cell Biol.* **195,** 193–201 (2011).
42. Bremner, K. H. *et al.* Adenovirus transport via direct interaction of cytoplasmic dynein with the viral capsid hexon subunit. *Cell Host Microbe* **6,** 523–535 (2009).

© 2014 Macmillan Publishers Limited. All rights reserved.

DOI: 10.1038/ncb3063

METHODS

Protein purification and characterization. All p150^{Glued} constructs for recombinant protein expression were cloned from full-length rat cDNA (EDL91133.1). p150^{Glued} CC1, CC1B, CC1A and p135-CC1 were cloned with C-terminal Flag and 6X His tags into pGEX 6P-1 (Amersham Biosciences), which encodes an N-terminal GST tag (Fig. 1). Proteins were expressed in BL21-CodonPlus RIPL competent cells (Agilent Technologies, #230280) with 0.5 mM IPTG for 4–6 h at 20 °C. Bacterial pellets were lysed in PBS with 1 mM dithiothreitol and 1:500 protease inhibitor cocktail (Sigma, P8340) by sonication and centrifuged at 4 °C for 30 min at 150,000*g* with a final concentration of 1% Triton-X. Proteins were purified with glutathione beads (GE, 17-0756-01) for 1 h at 4 °C. Washed beads were incubated overnight at 4 °C with Precission Protease (GE, 27-0843-01) in cleavage buffer (50 mM Tris-HCl pH 7.0, 150 mM NaCl, 1 mM EDTA) supplemented with 1 mM dithiothreitol to remove the GST tag. Proteins were supplemented with 5% glycerol, flash frozen and stored at −80 °C. p150 1–555 was expressed using the BaculoDirect System (Invitrogen). p150 1–555–Flag–6X His was cloned into entry vector pENTR1A (Invitrogen) and recombined with linear BaculoDirect. SF9 insect cells (Invitrogen, 11496-015) were infected with the recombination product a single population of virus was isolated by plaque assay. SF9 cells were infected for 48 h, and collected in lysis buffer (50 mM NaH_2PO_4, 300 mM NaCl, 10 mM imidazole) with 1:100 protease inhibitor cocktail and 1% IGEPAL CA-630 (Sigma I-3021). Cleared lysate was incubated with NTA-Nickel beads (Qiagen, 1018611) for 1 h at 4 °C, washed with lysis buffer containing 40 mM imidazole and protein was eluted in lysis buffer containing 250 mM imidazole. Buffer was exchanged to cleavage buffer using NAP columns (GE Healthcare) and protein was supplemented with 5% glycerol, flash frozen and stored at −80 °C. Full-length *Drosophila* kinesin was purified from wild-type *Drosophila* as in ref. 43. Bovine brain cytoplasmic dynein was purified as described previously[44] except that whole brains were flash frozen and stored at −80 °C before purification.

To analyse protein interactions, p150^{Glued} fragments were tested for dynein binding by immunoprecipitation with anti-flag antibody in PEM-35 (35 mM PIPES, 5 mM $MgSO_4$, 1 mM EGTA, 0.5 mM EDTA, pH 7.0) supplemented with 0.05–1 μg μl^{-1} BSA + 1 mM dithiothreitol + 0.1% Tween for 1–2 h at 4 °C with protein A beads (Invitrogen). Microtubule sedimentation assays were performed as follows. Purified bovine dynein (8 nM) mixed with 10× p150 fragment and 2.5 μM taxol-stabilized microtubules (Cytoskeleton, TL238) with or without 10 mM ATP (Sigma, A9187) in BRB80 (80 mM K-PIPES pH 6.9, 1 mM $MgCl_2$, 1 mM EGTA) supplemented with 20 μM taxol, 1 mM dithiothreitol and 0.05 μg μl^{-1} BSA was incubated for 30 min at room temperature, and centrifuged for 45 min at 35,000*g*. Supernatants and pellets were analysed by western blotting. Bacterially expressed CC1B was tested for an interaction with CC1A by pulldown with either GST–CC1A or GST alone in 20 mM Tris-HCl, pH 7.0 plus 40 mM NaCl, 1 mM EDTA, 0.1% Tween 20, 1 mM dithiothreitol, and protease inhibitor cocktail (Sigma) at 4 °C. Size-exclusion FPLC was performed using a 24 ml Superose 6 column pre-equilibrated with 20 mM Tris-HCl, pH 7.0, containing 1 mM EDTA at 4 °C. Immunoprecipitation and/or blotting antibodies used are: anti-alpha tubulin (Sigma, T9026 used at 1:10,000 for blotting) 74.1 anti-dynein intermediate chain (gift from K. Pfister used at 1:5,000 for blotting), anti-Flag (Sigma, F1804 M2 used at 1:10,000 for blotting), anti-DDDDK (Abcam ab1162 used at 1:40 for immunoprecipitation) and anti-dynein heavy chain (used at 1:1,000 for blotting)[45].

To assess protein folding, we used circular dichroism. All proteins were dialysed overnight into 50 mM sodium phosphate buffer, pH 7.0, and circular dichroism measurements were taken on a Jasco-J815 spectrapolimeter. Fixed-temperature measurements were collected in 0.1 mm cuvettes at 185–260 nm wavelengths, 0.1 nm data pitch, continuous scanning mode, at standard sensitivity, with a scanning speed of 50 nm min^{-1}, response of 8 s, and bandwidth of 1 nm. For each sample 3 data sets were accumulated per run. Melting curve data were accumulated at 222 nm from 5 to 85 °C (for CC1) and 5–60 °C (for CC1B) in a 1 mm cuvette with a data pitch of 0.5 °C, a 10 s delay, a temperature slope of 40 °C h^{-1}, standard sensitivity, 8 s response and a bandwidth of 1 nm. The cooling curve was collected in the same manner reversing the temperature 15 s after reaching the maximum. Molar ellipticities were calculated as described previously[46,47]. Secondary structure content predictions were made using the online server DICHROWEB (http://dichroweb.cryst.bbk.ac.uk/html/home.shtml). For comparison, the online server COILS (http://embnet.vital-it.ch/software/COILS_form.html) was used to predict coiled-coil structure from the amino-acid sequences.

***In vitro* optical bead assay.** Optical-trapping motility assays, data recording, particle tracking and stalling-force analysis were performed as previously described[48], with the exception of the new implementation of force-feedback as described below.

For single-molecule dynein assays, a 489-nm-diameter carboxylate polystyrene bead (Poly-sciences, catalogue no. 09836-15), with nonspecifically attached motors, was positioned in a flow chamber above a taxol-stabilized microtubule for 30 s to allow for binding. The single-motor range was attained when the percentage of beads binding is smaller than or equal to 30% (ref. 49). For run-length measurements of single dynein, a run was defined as the distance travelled from initial binding until the bead detached (with optical trap turned off). The distribution of run lengths was fitted to a single exponential decay to obtain mean run length and associated uncertainty. For processivity measurements, we made measurements on at least 40–50 beads with active motors. For each run, velocity was obtained by dividing run length by the duration of the run. The mean velocity and associated uncertainty was calculated from a statistical average of all velocities. We define the stall force (F_s) as the mean value of the load force at which the motor stops moving. Stall force measurements of single dynein beads were made with a trap stiffness of 1.5 pN per 100 nm. An event was classified as a stall when a single-motor bead moved away from the trap centre and held its plateau position with a velocity of <10 nm s^{-1} for $\geq$100 ms before detachment. The mean stall force (and s.e.m.) were calculated from the Gaussian peak position (and uncertainty) of the stall-force distribution. For force measurements, we made measurements with at least 40–50 beads with active motors. The obtained decay constant and uncertainty presented in each plot represents the average detachment time and s.e.m. respectively. Statistical significance was determined using Student's *t*-test. To determine the overall frequency of diffusive versus processive motion (for example, in experiments summarized in Fig. 3), we ultimately looked at 50–60 independent beads that had microtubule-binding activity. As the binding fraction was ∼30%, this required experiments on roughly 150–200 independent beads chosen randomly in solution. All summarized bead experiments were replicated at least 3 times, but usually more.

For single-molecule bead assay of dynein with p150^{Glued} fragments, dynein was adsorbed onto carboxylate beads, which were then blocked with casein (10 mM) and subsequently exposed to a 150-fold molar excess of p150^{Glued} fragment. Excess dynein and fragments were removed by gentle centrifugation. Optical trap bead assays were performed in dynein motility buffer (35 mM PIPES pH 7.0, 5 mM $MgSO_4$, 1 mM EGTA, 0.5 mM EDTA) in the presence of 1 mM ATP and an oxygen scavenging system (250 μg ml^{-1} glucose oxidase, 30 μg ml^{-1} catalase, 4.6 mg ml^{-1} glucose[50]).

We quantified the amount of diffusive versus processive dynein. We (see, for example, Fig. 6 in ref. 51) and others[24,26] have in the past reported that dynein can be in both diffusive and processive states. The likelihood of diffusive events decreases when more motors are present on the bead[51]. Experiments are performed on microtubule-purified dynein (before experiments, a microtubule-pelleting/release step selects for active dynein). At the single-molecule level the percentage of processive versus diffusive beads can vary between different purifications (although not among multiple aliquots from the same original purification): typically ∼25% of tested beads show processive motion, and 5% show diffusive motion (Fig. 3d). Thus, roughly 83% of binding events are processive, and 17% diffusive. If the dynein is aged (on ice, 4 °C, for 2–3 days) the diffusive fraction increases to ∼40%. Some purifications show significantly more diffusive events from the start; we typically do not use those. The studies in this paper reflect the use of bovine dynein from 3 to 4 independent purifications. In the experiments to assess effects of dynactin fragments on dynein's diffusion, we always do the experiment and the control on the same day, using the same dynein aliquot, with experiments interspersed.

To determine whether there was any remaining force production by diffusive beads, we compared the motion of beads diffusing owing to the p150^{Glued} 1–555 fragment alone (lacking motors) with the other diffusing dynein–dynactin fragment beads, in each case monitoring the position of the bead in the optical trap, originally sampled at 4 kHz, and subsequently averaged to 1 kHz to decrease noise. These traces were then analysed using Kerssemakers's step-detection algorithm. The detected steps were restricted with a condition of waiting time $\geq$50 ms, and the distribution of forces at which the bead survives with this condition was obtained.

To allow determination of the step-size distribution, we needed to use a force-feedback set-up. For step-size measurements at saturating ATP concentrations, we used an optical trap with force feedback to suppress thermal noise; the trap moved to follow the bead and minimize opposition to motion. High temporal and spatial resolution measurements were made using a laser to detect the bead's location.

The experimental set-up and calibration was done as in ref. 52 augmented by an acousto-optic deflector (AOD) to allow force-feedback. Video tracking of a trapped bead in two dimensions was used to obtain the conversion parameters from AOD drive frequency (megahertz) to position (nanometres). Trap stiffness was calibrated using quadrant photodiode signals with the power-spectrum method. With the AOD, the trap stiffness perpendicular to the microtubule (*y*-direction) is $<$20% smaller than the trap stiffness parallel to the microtubule (*x*-direction). The calibration of trap stiffness was confirmed by measuring kinesin stall forces with and without the AOD. As trap stiffness along the microtubule was constant up to 2 μm from the centre, all step-size measurements were made within ±1.5 μm from the centre to maintain constant trap stiffness. The trap stiffness was 1.5 pN/100 nm, so the maximum force the bead stepped against was lower, and dependent on step size. For example, a 16-nm-step attempt, starting at 24 nm from the trap centre and ending at 40 nm, would experience 0.36 pN of load. Using this system we measured

© 2014 Macmillan Publishers Limited. All rights reserved.

rapidly stepping single motors attached to beads undergoing a low force opposing motion. The quadrant photodiode signal was obtained at a scanning rate of 4 kHz and AOD feedback occurred every 40 nm (the largest dynein step size possible) of bead displacement from the centre of the trap, to maintain the bead at the centre of the laser. This signal was averaged to 1 kHz, and analysed for steps within each 40 nm stationary period using Kerssemakers's step-detection algorithm[53].

As part of our step-size analysis, we used theoretical simulations. Rapid sequential steps of potentially varying size can be 'fused' together by the step-detection procedure, resulting in 'detection' of excessive large steps[54]. To address this confounding issue, we developed a partly synthetic data approach, as done previously in another context[55].

Theoretically simulated motion was combined with experimentally measured noise to generate simulated tracks that were then analysed for stepping. Programs to generate simulated tracks for step detection were developed using self-written Matlab codes. The tracks comprised a known percentage of steps with given step sizes, with a mean dwell time between steps derived from a decaying exponential distribution. The mean dwell time was chosen to match experimentally determined velocities, taking into account the distribution of step sizes and the percentage of forward and backward steps. The tracks were generated at 4 kHz as measured in the experiment. Experimentally measured noise, generated from beads tethered to microtubules through non-stepping dynein (in the absence of ATP) with the trap feedback engaged, was added to the simulated tracks, which were then averaged to 1 kHz and analysed using step detection. The step-size distributions were normalized to the total number of steps (to avoid the effect of data size) and compared to the experimental step-size distribution by calculating the residual, which is the difference between the two normalized step-size distributions. Smaller residuals indicated better agreement between the two. Simulated distributions were adjusted to minimize the residual and determine the correct experimental distribution.

We confirmed this method by measuring kinesin's step distribution, which is comprised of predominately 8-nm plus-end-directed steps with occasional backward steps[56] (Supplementary Fig. 4A–E).

For dynein, experimental trajectories were derived from beads driven by single dyneins with or without CC1B moving at ~400 nm s^{-1} with saturating (1 mm) ATP.

To detect lateral motion and determine the size of lateral steps, we used video-enhanced DIC microscopy, coupled with sub-pixel-resolution particle tracking[57] to analyse lateral motion. As a control, kinesin was first tested as follows. The distributions of motion for 200-nm-diameter carboxylate beads with single-molecule concentrations of kinesin either tethered to the microtubule (in the presence of AMP-PNP) or moving freely along the microtubule (with 1 mM ATP) were measured (Supplementary Fig. 5C,D). We projected the bead's motion along the microtubule onto the best-fit line trajectory, and determined the Y-bead position (perpendicular to the microtubule). Protofilament switching events were detected by analysing traces using step detection. Experiments were done at ~30% binding fraction to ensure single kinesin or dynein activity, with the trap turned off to allow free lateral motion.

43. Sigua, R., Tripathy, S., Anand, P. & Gross, S. P. Isolation and purification of kinesin from *Drosophila* embryos. *J. Vis. Exp.* (2012).
44. Paschal, B. M., Shpetner, H. S. & Vallee, R. B. Purification of brain cytoplasmic dynein and characterization of its *in vitro* properties. *Methods Enzymol.* **196,** 181–191 (1991).
45. Mikami, A. *et al.* Molecular structure of cytoplasmic dynein 2 and its distribution in neuronal and ciliated cells. *J. Cell Sci.* **115,** 4801–4808 (2002).
46. Bohm, K. J., Stracke, R. & Unger, E. Speeding up kinesin-driven microtubule gliding *in vitro* by variation of cofactor composition and physicochemical parameters. *Cell Biol. Int.* **24,** 335–341 (2000).
47. Kelly, S. M., Jess, T. J. & Price, N. C. How to study proteins by circular dichroism. *Biochim. Biophys. Acta* **1751,** 119–139 (2005).
48. Kunwar, A. *et al.* Mechanical stochastic tug-of-war models cannot explain bidirectional lipid-droplet transport. *Proc. Natl Acad. Sci. USA* **108,** 18960–18965 (2011).
49. Svoboda, K. & Block, S. M. Force and velocity measured for single kinesin molecules. *Cell* **77,** 773–784 (1994).
50. Vershinin, M., Carter, B. C., Razafsky, D. S., King, S. J. & Gross, S. P. Multiple-motor based transport and its regulation by Tau. *Proc. Natl Acad. Sci. USA* **104,** 87–92 (2007).
51. Mallik, R., Petrov, D., Lex, S. A., King, S. J. & Gross, S. P. Building complexity: an *in vitro* study of cytoplasmic dynein with *in vivo* implications. *Curr. Biol.* **15,** 2075–2085 (2005).
52. Lang, M. J., Asbury, C. L., Shaevitz, J. W. & Block, S. M. An automated two-dimensional optical force clamp for single molecule studies. *Biophys. J.* **83,** 491–501 (2002).
53. Kerssemakers, J. W. *et al.* Assembly dynamics of microtubules at molecular resolution. *Nature* **442,** 709–712 (2006).
54. Carter, B. C., Vershinin, M. & Gross, S. P. A comparison of step-detection methods: how well can you do? *Biophys. J.* **94,** 306–319 (2008).
55. Pearson, C. G. *et al.* Measuring nanometer scale gradients in spindle microtubule dynamics using model convolution microscopy. *Mol. Biol. Cell* **17,** 4069–4079 (2006).
56. Carter, N. J. & Cross, R. A. Mechanics of the kinesin step. *Nature* **435,** 308–312 (2005).
57. Carter, B. C., Shubeita, G. T. & Gross, S. P. Tracking single particles: a user-friendly quantitative evaluation. *Phys. Biol.* **2,** 60–72 (2005).

© 2014 Macmillan Publishers Limited. All rights reserved.

DOI: 10.1038/ncb3063

nature cell biology

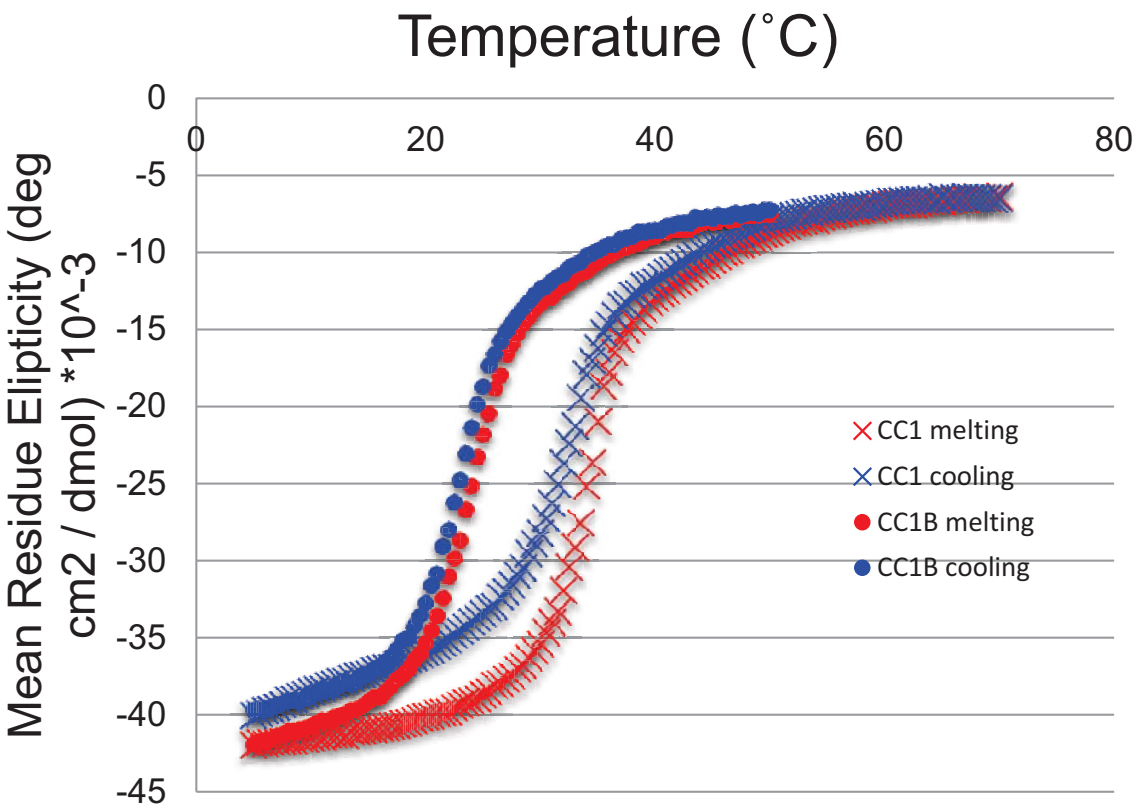

Supplementary Figure 1 Temperature dependent melting and reannealing of p150^{Glued} CC1 and CC1B fragments. Molar ellipticity of CC1 and CC1B at 222 nm was monitored under increasing and decreasing temperature. Unfolding was reversible. T_m values were 23.5˚C for CC1B and 33˚C for CC1. (One independent experiment).

© 2014 Macmillan Publishers Limited. All rights reserved.

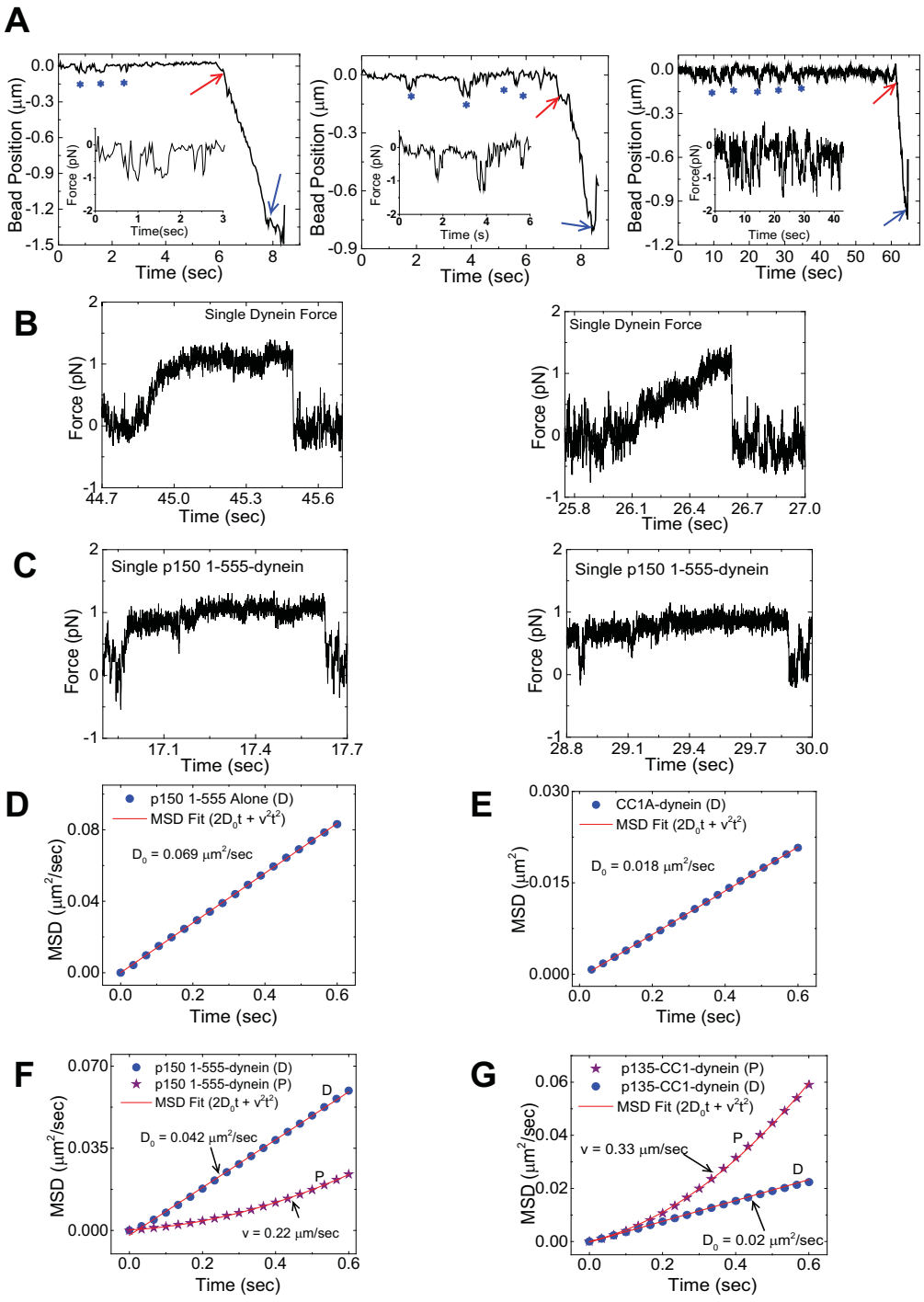

Supplementary Figure 2 Additional examples of force traces and MSD curves. (A) Video trace showing measurement of single dynein force followed by its run-length. Blue star marks force production, red arrow indicates turning off of optical trap, and blue arrow shows end of runlength (B) and (C): Force traces from dynein alone and with P150. Experiments were done at a bead binding fraction of 30%. (D): The MSD curve for beads with P150 alone (30% binding fraction) diffusing along microtubules. (E) The MSD curve for single-molecule dynein beads (30% bf) with CC1A, diffusing along MTs. (F, G): MSD curves for dynein (again 30% bf) with P150 (E) and P135 (F). The blue curves reflect the diffusing beads, whereas the red curves reflect the processively moving beads.

© 2014 Macmillan Publishers Limited. All rights reserved.

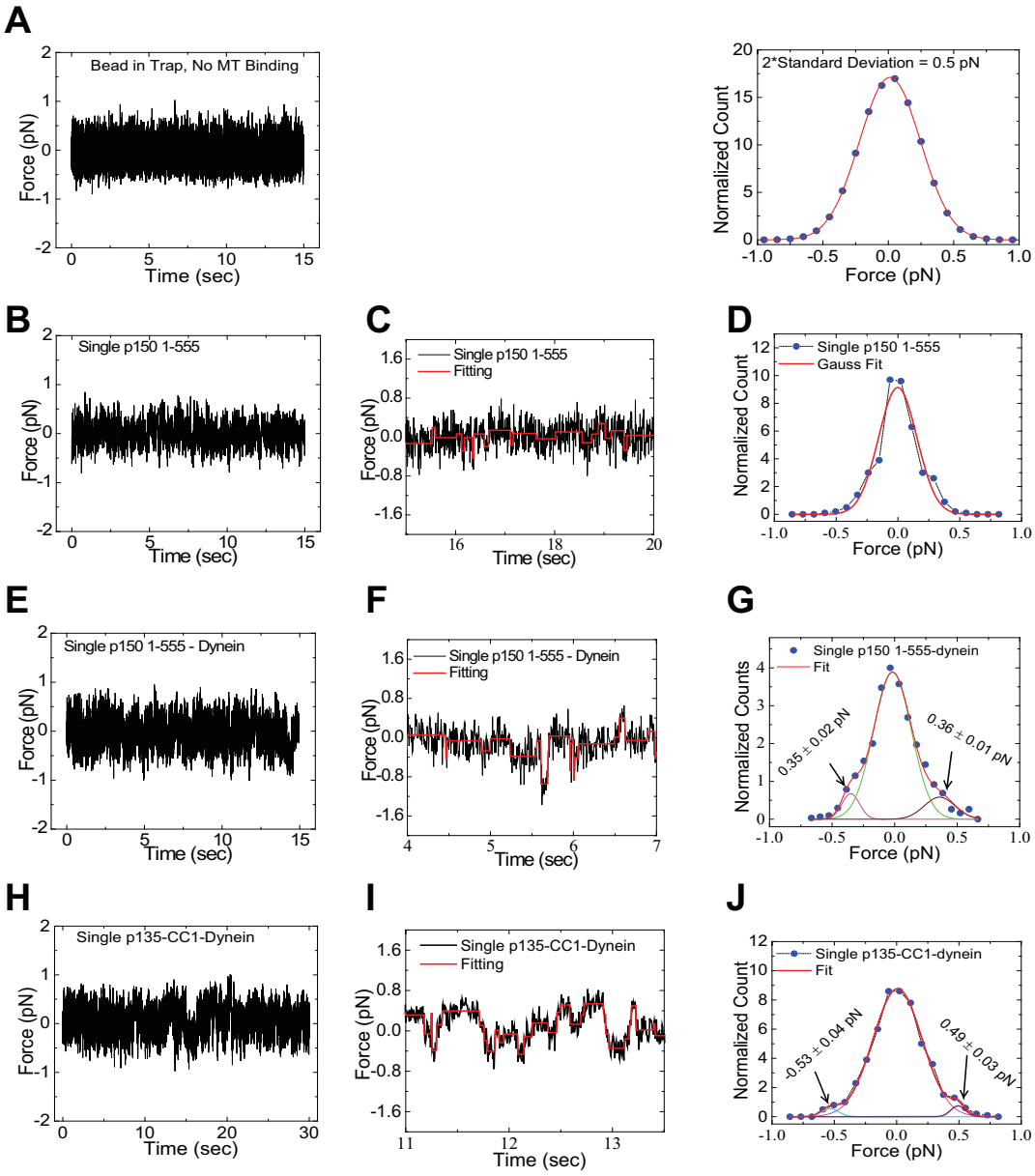

Supplementary Figure 3 Measurement of force distribution for diffusive beads. (A) (left):Force trace of free bead, held in trap. The quadrant photo diode (QPD) signal was obtained at 4 KHz, with trap stiffness of 1.5 pN/100nm. (right):histogram of detected forces due to thermal motion for the free bead (B) Force trace for bead attached to microtubule by a single p150 1-555 without dynein. (C) Higher temporal resolution image of (B). (D) Distribution of displacements (from fits in (B)) from many traces (475 force events). (E, F, and G (775 force events) Same as (A, B and C) for, dynein with p150 1-555. (H, I and J (518 force events)) Same as (A, B and C) for dynein with p135-CC1. In all cases, the QPD signal was averaged to 1 KHz and analyzed using Kerssemakers' step detection algorithm, with waiting time restricted to ≥ 50 ms. While (D) is described by a single Gaussian (no additional force production), (G) and (J) each require the sum of three Gaussian peaks. The small peaks indicate the presence of some force. We interpret these small forces as likely reflecting transient binding/release events by dynein (see supplemental discussion).

© 2014 Macmillan Publishers Limited. All rights reserved.

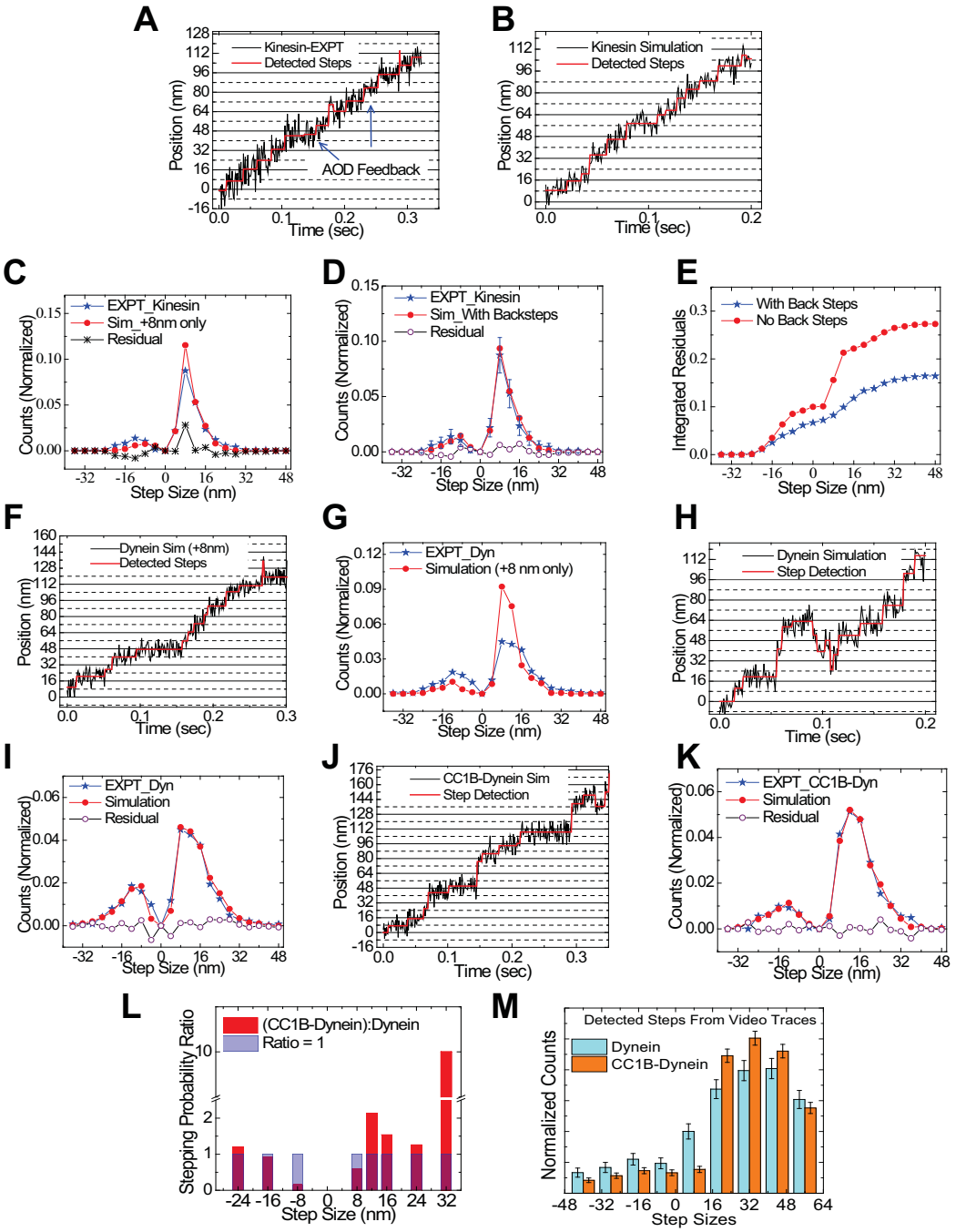

Supplementary Figure 4 Characterization of step detection. Step sizes were measured with an optical trap and an acousto optic deflector (AOD) force feedback system on single-motor (30% binding fraction) beads. The bead was maintained at the trap center by AOD feedback every 40 nm (blue arrows in A). (A) A trace with detected steps (in red) for single kinesin moving at a velocity similar to dynein (500 nm/sec). (B, F, H and J) Simulated tracks with detected steps for kinesin (309 steps), dynein with 8nm steps only, dynein (number of steps = 659) and CC1B-dynein (428 steps). (C, D, G, I and K) Step size distributions determined from experiment (blue star, real tracks such as in Fig. 3A and B) and simulated tracks with real noise (red circles) for single-molecule kinesin with plus end directed 8 nm steps only, kinesin involving back-steps, dynein with minus end directed 8 nm steps only and for single dynein with and without CC1B (405 steps used in K). Purple open circles are the residual, indicating difference between distributions. (E) Integrated residual from (C) and (D) is smaller when back-steps are for kinesin are included. (L) Normalized step probability for dynein with and without CC1B. (M) Steps were detected from video tracking traces (48 traces) of moving beads coated with dynein or dynein/CC1B (30 frames/sec) without force feedback. Step distributions are in qualitative agreement with step detection from AODs.

© 2014 Macmillan Publishers Limited. All rights reserved.

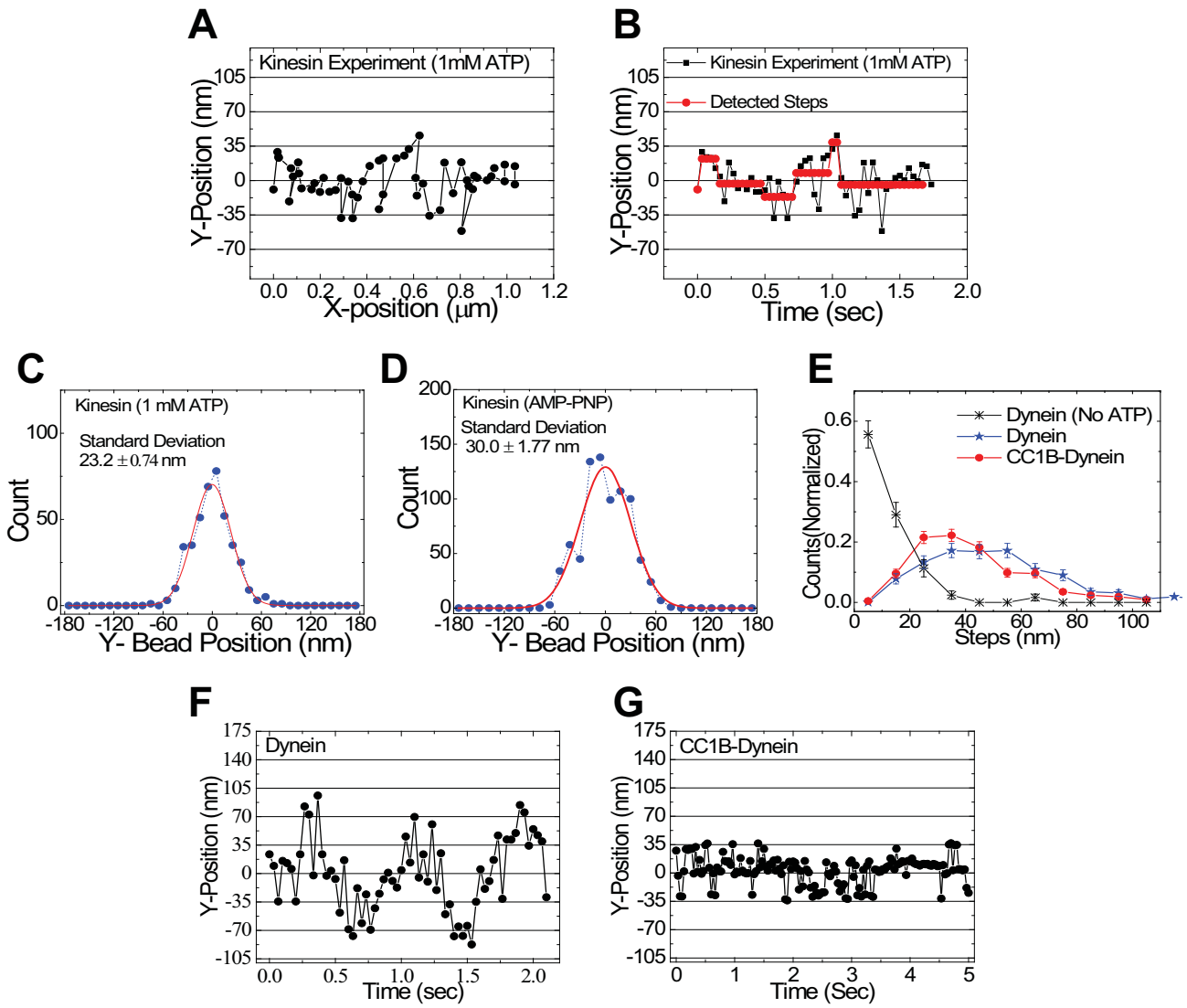

Supplementary Figure 5 Characterization of lateral motion. Beads with adsorbed kinesin, dynein, or dynein plus the p150^{Glued} CC1B fragment were analyzed for bead motion perpendicular to the microtubule long axis (Y- bead position). (A) Example traces of Y-bead position vs. time for kinesin at saturating ATP. (B) Detected steps (red lines) from (A). (C) Gaussian distribution of detected steps (25 processive bead). (D) Lateral step size distribution of kinesin in the presence of AMP-PNP (20 beads checked). Distributions in (C) and (D) are similar indicating that kinesin does not take lateral steps. (E) Lateral step size distributions of dynein without ATP (black) or dynein (blue), and dynein with CC1B (red) with saturating ATP (428 lateral steps). (F and G) are example traces of Y-FLOP of bead for dynein and CC1B-dynein.

© 2014 Macmillan Publishers Limited. All rights reserved.

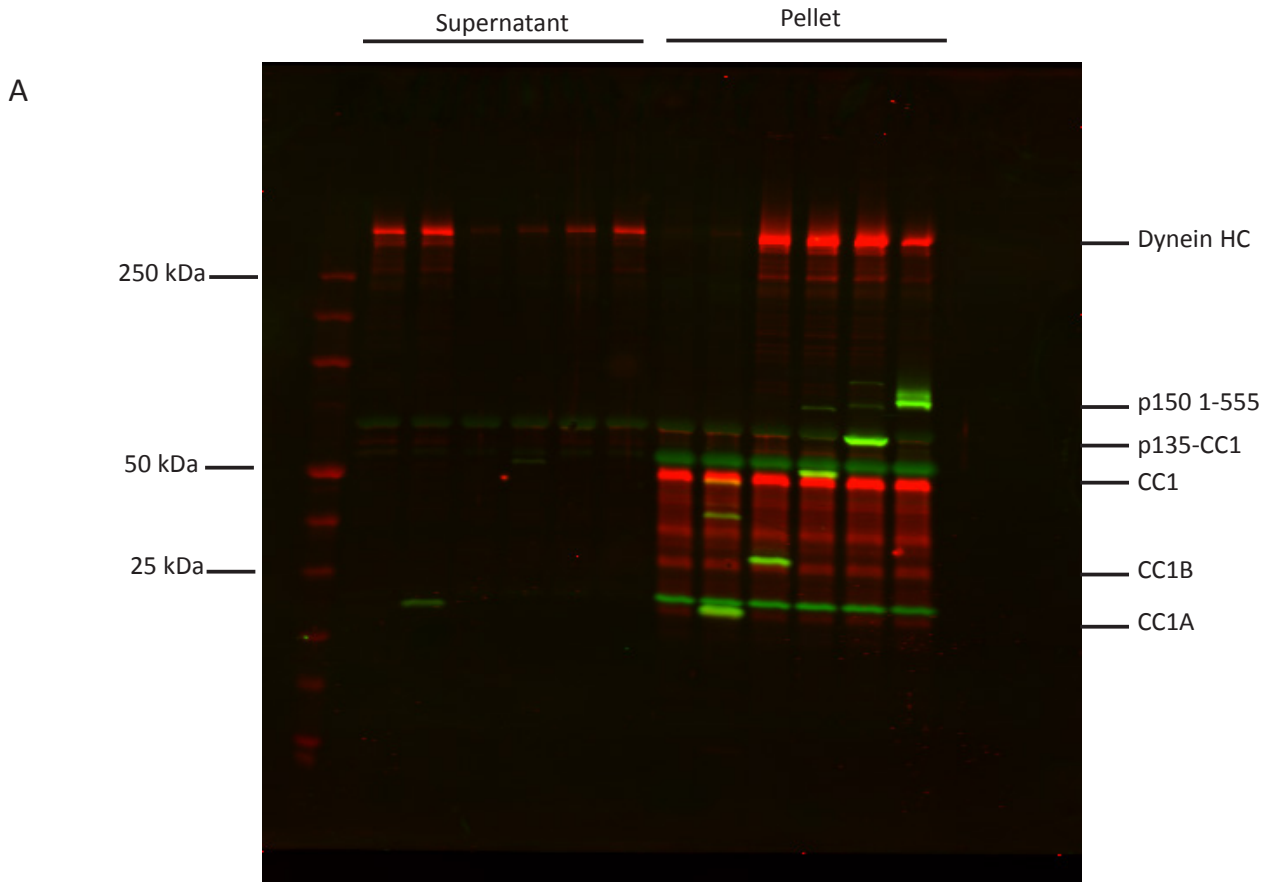

Full scan for Fig 1D

Supplementary Figure 6 Full scans of immunoblots and gels from Fig. 1 and Fig. 6. A) Full scan for Fig. 1D. B) Full scan for Fig. 1E panel 1. (C) Full scan for Fig. 1E, panels 2-4. (D) Full scan for Fig1E, panel 5. (E) Full scan for Fig. 6A. (F) Full scan for Fig 6B, upper panel. (G) Full scan for Fig. 6B, middle panel. (H) Full scan for Fig. 6B, lower panel.

© 2014 Macmillan Publishers Limited. All rights reserved.

B

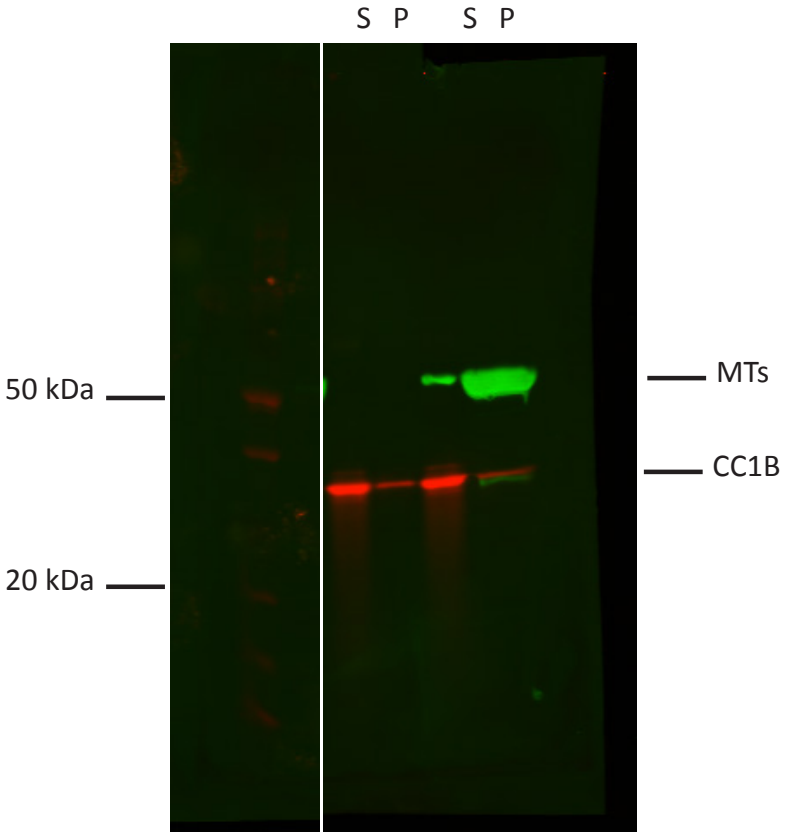

Full scan for Fig 1E panel 1

Supplementary Figure 6 continued

© 2014 Macmillan Publishers Limited. All rights reserved.

C

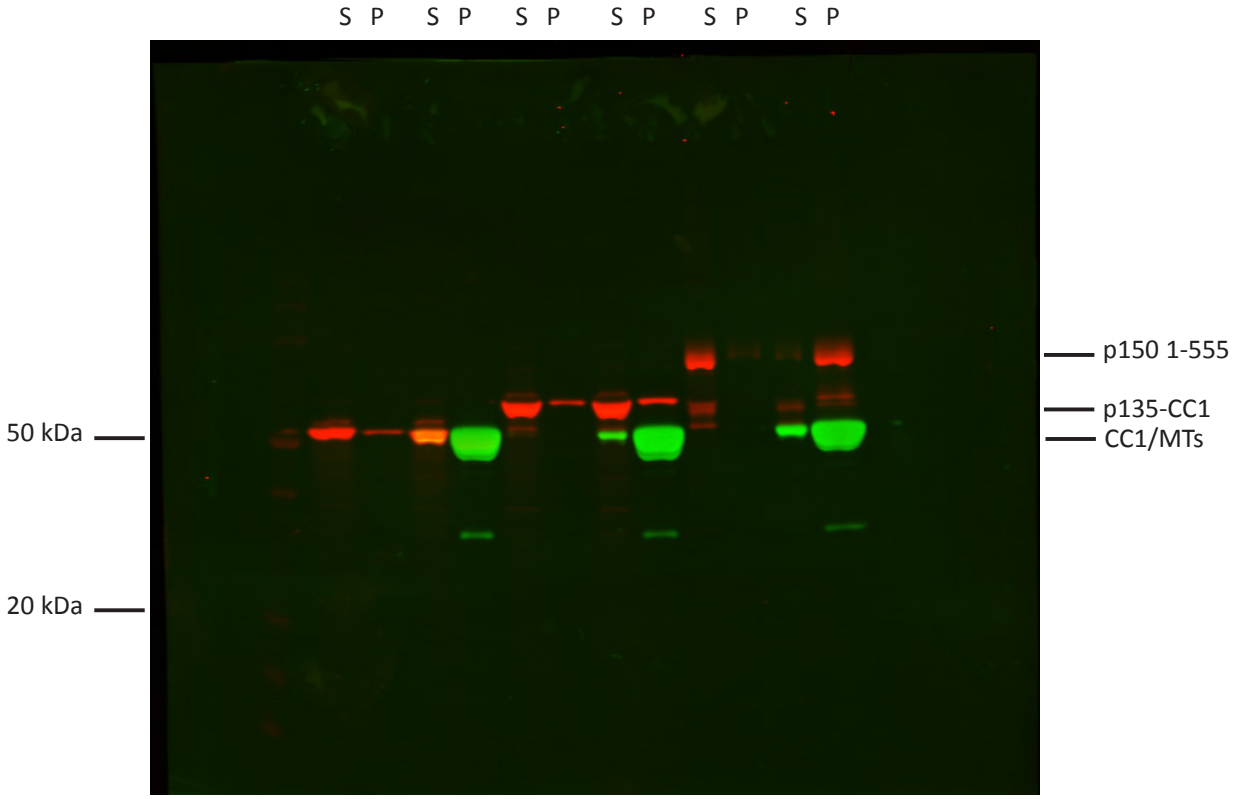

Full scan for Fig 1E panels 2-4

Supplementary Figure 6 continued

© 2014 Macmillan Publishers Limited. All rights reserved.

D

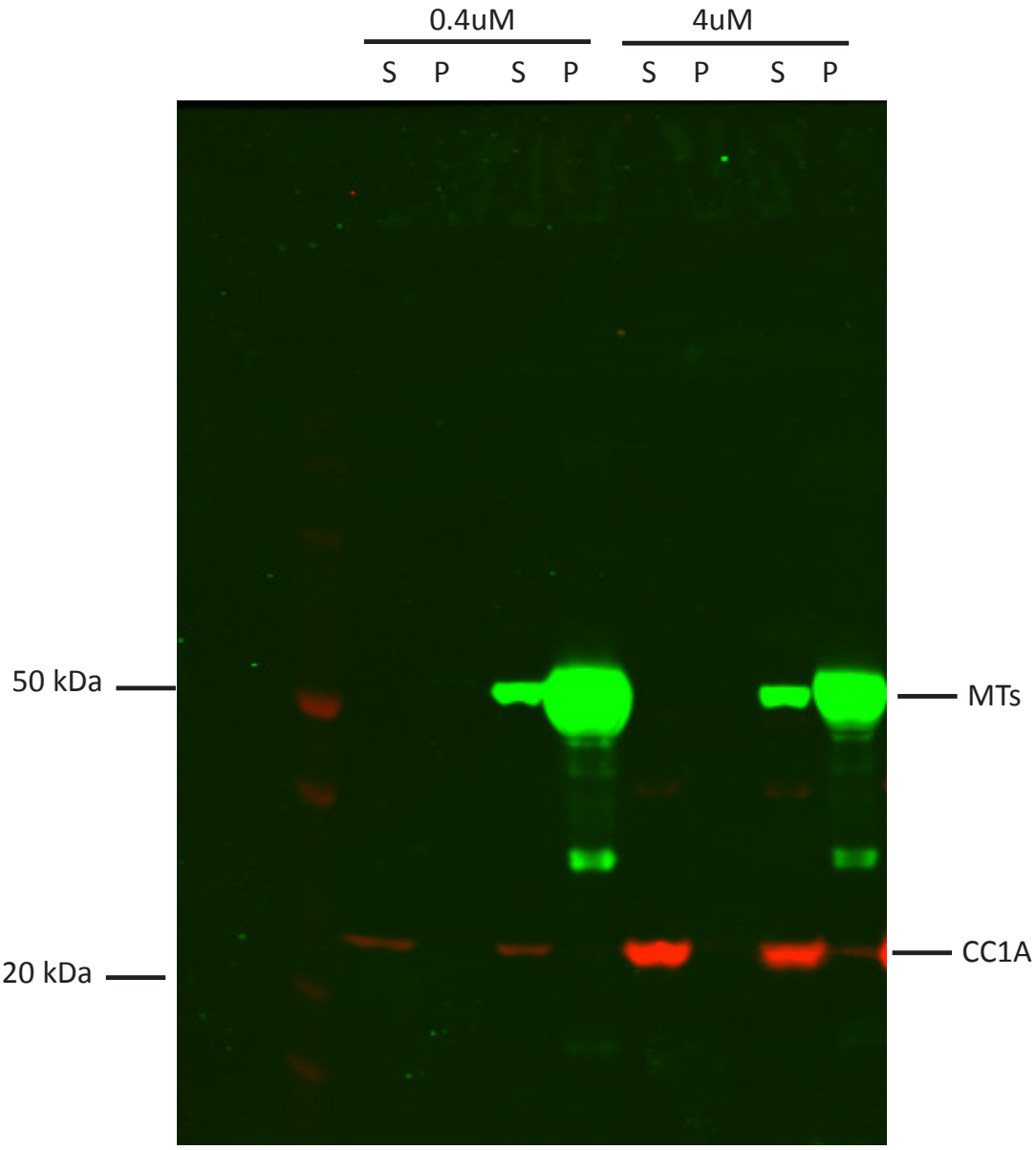

Full scan for Fig 1E panel 5

Supplementary Figure 6 continued

© 2014 Macmillan Publishers Limited. All rights reserved.

E

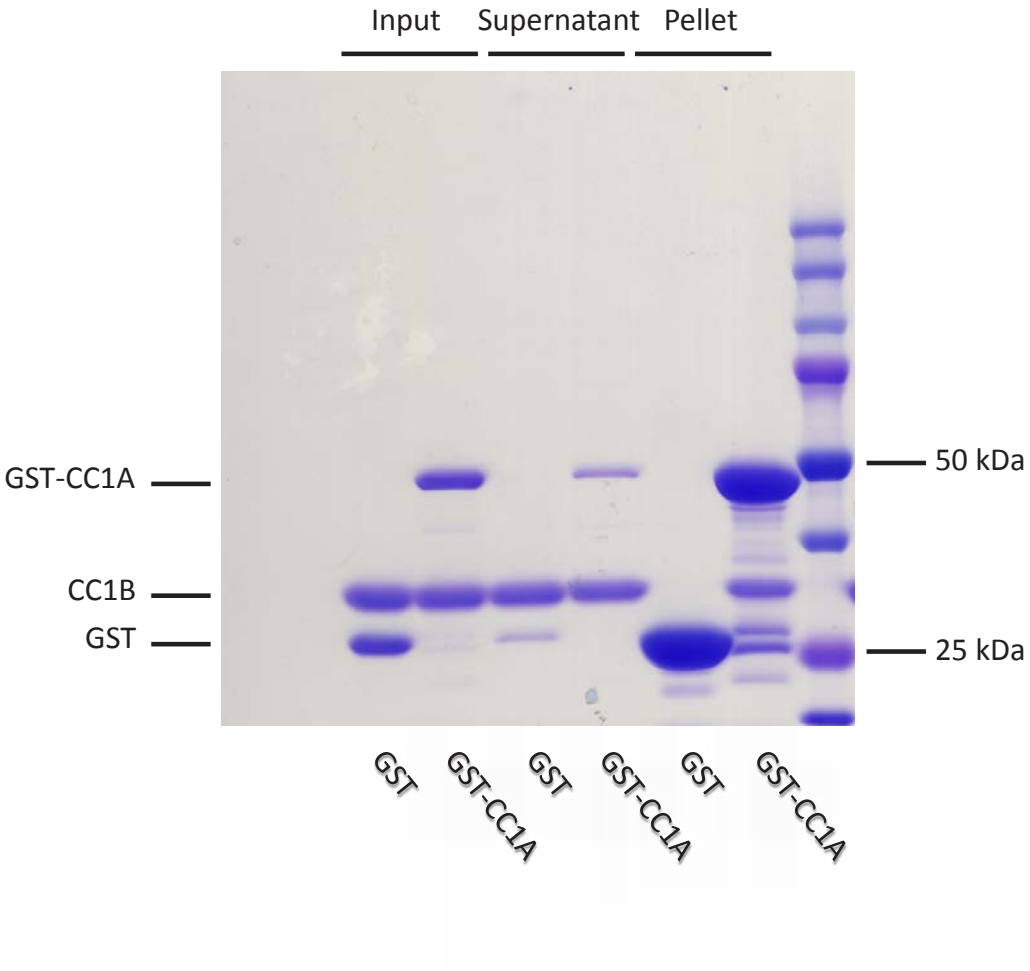

Full scan for Fig 6A

Supplementary Figure 6 continued

© 2014 Macmillan Publishers Limited. All rights reserved.

F

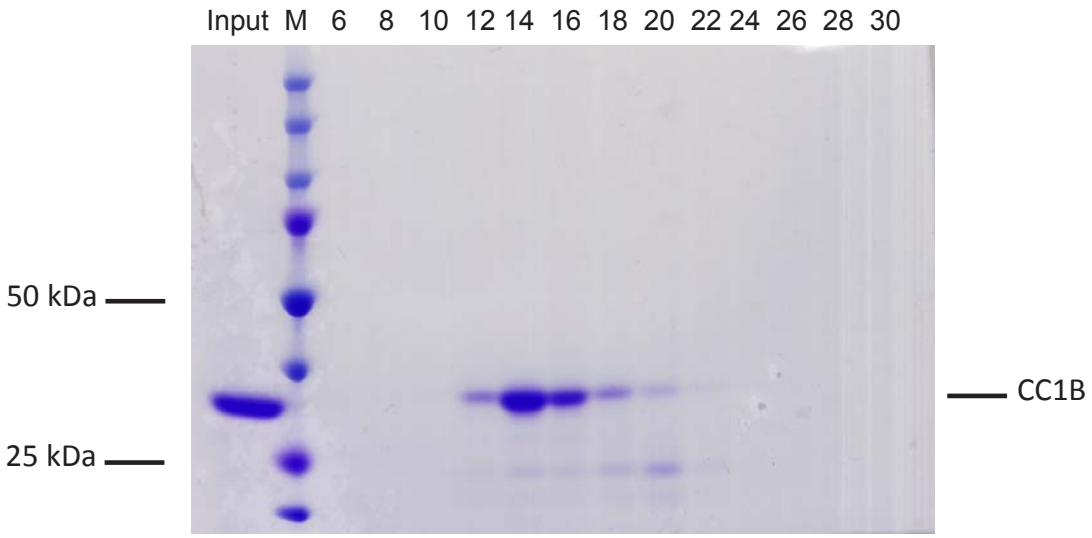

Full scan for Fig 6B upper panel

Supplementary Figure 6 continued

© 2014 Macmillan Publishers Limited. All rights reserved.

G

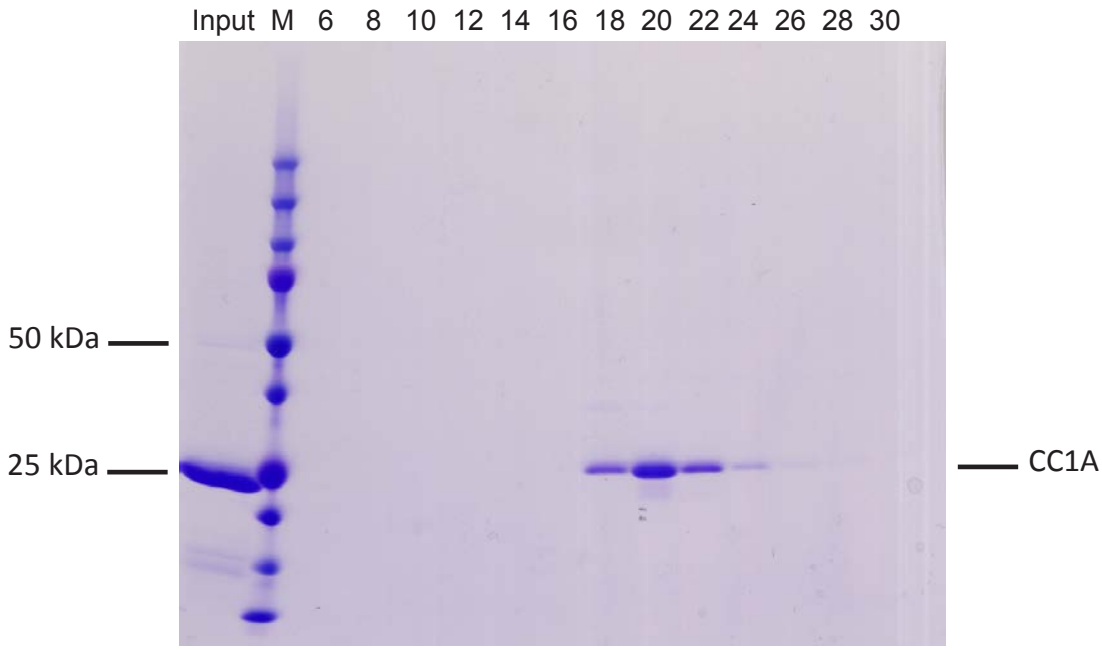

Full scan for Fig 6B middle panel

Supplementary Figure 6 continued

© 2014 Macmillan Publishers Limited. All rights reserved.

H

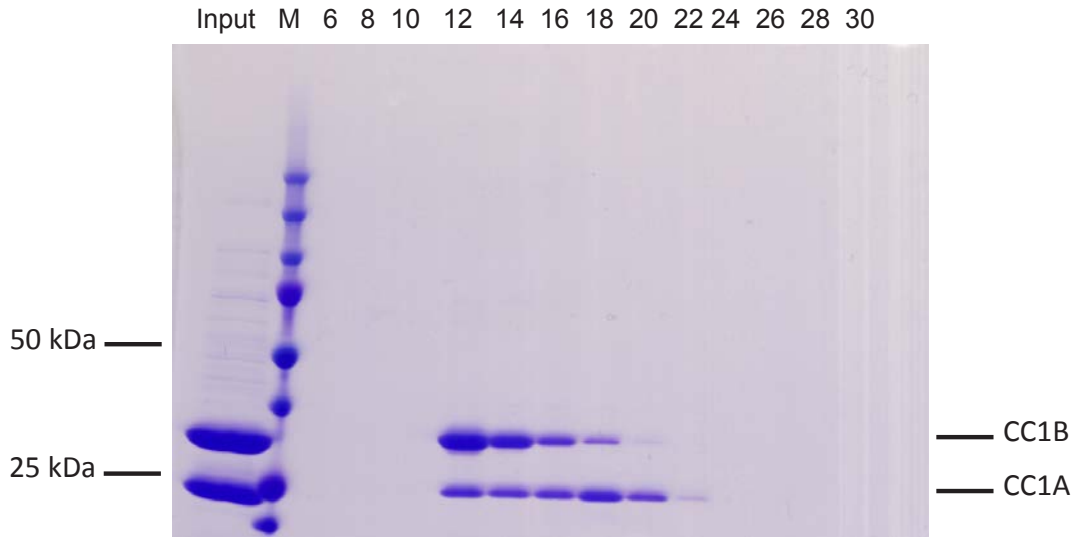

Full scan for Fig 6B lower panel

Supplementary Figure 6 continued

© 2014 Macmillan Publishers Limited. All rights reserved.

4˚C	Alpha Helices	Beta Strands	Turns/ Unordered	Θ222/Θ208
CC1	0.984	0.016	0	1.116
CC1B	0.981	0.019	0	1.115
CC1A	0.983	0.017	0	1.090
p135 CC1	0.944	0.022	0.034	1.027
1-555	0.355	0.148	0.497	0.961

25˚C	Alpha Helices	Beta Strands	Turns/ Unordered	Θ222/Θ208	predicted coiled-coil content
CC1	0.975	0.015	0.01	1.075	0.924
CC1B	0.975	0.015	0.01	1.050	0.952
CC1A	0.974	0.012	0.013	1.016	0.865
p135 CC1	0.94	0.024	0.035	1.008	0.758
1-555	0.361	0.152	0.487	0.970	0.582

37˚C	Alpha Helices	Beta Strands	Turns/ Unordered	Θ222/Θ208
CC1	0.665	0.031	0.304	0.964
CC1B	0.359	0.05	0.591	0.650
CC1A	0.579	0.026	0.394	0.814
p135 CC1	0.944	0.022	0.034	0.956
1-555	0.318	0.161	0.52	0.892

Supplementary Table 1 Summary of circular dichroism (CD) data for p150^{Glued} fragments. The fraction α-helix, β-sheet, or disordered structure for each fragment was calculated from molar ellipticities measured at 4, 25 and 37˚C. A ratio of molar ellipticities θ_{222} / θ_{208} >1 indicates coiled-coil α-helical structure. Predicted coiled-coil α-helical content was determined with COILS. CD data for the shorter fragments corresponded well with predicted coiled-coil content. p135-CC1 showed more α-helical content than is predicted to form from the coiled-coil region, suggesting N-terminal regions are α-helical. In contrast, p150^{Glued} 1-555 showed less α-helical content, indicating that the coiled-coil region may be unfolded in this fragment.

© 2014 Macmillan Publishers Limited. All rights reserved.

Step Size (nm)	-32	-24	-16	-12	-8	8	12	16	24
Kinesin	0	0	0	0	5.5	94.5	0	0	0
Dynein	0.5	7.5	18.5	11	38	12.5	3	6.5	2.5
CC1B-Dynein	5	9.5	28.5	23.5	22.5	2	0	6	3

Supplementary Table 2 Stepping behavior summary for kinesin, dynein, and dynein + CC1B. Frequency of steps as a function of size. Step size was determined as described in Methods. (3 independent experiments were used to verify the reproducibility).

© 2014 Macmillan Publishers Limited. All rights reserved.